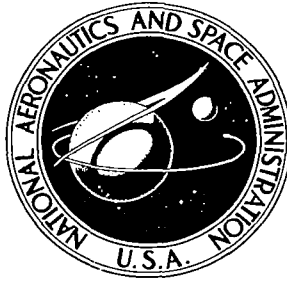


**NASA TECHNICAL
MEMORANDUM**



NASA TM X-2486

C. 1

NASA TM X-2486

**LOAN COPY: RETI
AFWL (DOU)
KIRTLAND AFB,**



**MULTIPLE-ORIFICE LIQUID INJECTION
INTO HYPERSONIC AIR STREAMS AND
APPLICATION TO RAM C-III FLIGHT**

*by William L. Weaver
Langley Research Center
Hampton, Va. 23365*

ERRATA

NASA Technical Memorandum X-2486

MULTIPLE-ORIFICE LIQUID INJECTION
INTO HYPERSONIC AIRSTREAMS AND APPLICATION
TO RAM C-III FLIGHT

By William L. Weaver
February 1972

Page 19, table I: The sixth item under "Nozzle patterns" for the flat-plate model should read as follows:

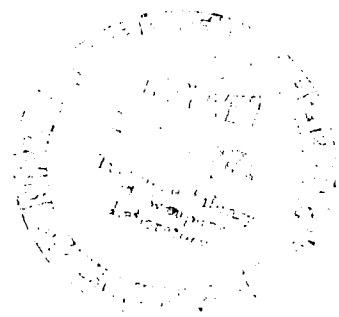
⑦ ⑦ ⑤ ⑤ ③ ③

Page 30, figure 7(b): The upper left photograph was inadvertently printed upside down. A corrected page 30 is attached.

Pages 33 and 35, figures 10(a) and 10(c): The two photographs on the right of each page of figures were inadvertently printed interchanged. Corrected pages 33 and 35 are attached.

Page 45, figure 14(f): The first equation in the notation under the top three photographs should be changed from $\bar{q}_\infty = 16.3 \text{ kN/m}^2$ to $q_\infty = 16.3 \text{ kN/m}^2$.

Issued October 1972



Errata inserted
1 Nov-72 JH



0151922

1. Report No. NASA TM X-2486	2. Government Accession No.	3. Recipient's Catalog No.	
4. Title and Subtitle MULTIPLE-ORIFICE LIQUID INJECTION INTO HYPERSONIC AIRSTREAMS AND APPLICATION TO RAM C-III FLIGHT		5. Report Date February 1972	6. Performing Organization Code
		8. Performing Organization Report No. L-8023	
7. Author(s) William L. Weaver		10. Work Unit No. 115-21-01-01	11. Contract or Grant No.
9. Performing Organization Name and Address NASA Langley Research Center Hampton, Va. 23365		13. Type of Report and Period Covered Technical Memorandum	
		14. Sponsoring Agency Code	
12. Sponsoring Agency Name and Address National Aeronautics and Space Administration Washington, D.C. 20546		15. Supplementary Notes	
16. Abstract <p>Experimental data are presented for the oblique injection of water and three electro-philic liquids (fluorocarbon compounds) through multiple-orifice nozzles from a flat plate and the sides of a hemisphere-cone (0.375 scale of RAM C spacecraft) into hypersonic air-streams. The nozzle patterns included single and multiple orifices, single rows of nozzles, and duplicates of the RAM C-III nozzles. The flat-plate tests were made at Mach 8. Total pressure was varied from 3.45 MN/m² to 10.34 MN/m², Reynolds number was varied from 9.84 × 10⁶ per meter to 19.7 × 10⁶ per meter, and liquid injection pressure was varied from 0.69 MN/m² to 3.5 MN/m². The hemisphere-cone tests were made at Mach 7.3. Total pressure was varied from 1.38 MN/m² to 6.89 MN/m², Reynolds number was varied from 3.54 × 10⁶ per meter to 17.7 × 10⁶ per meter, and liquid-injection pressure was varied from 0.34 MN/m² to 4.14 MN/m². Photographs of the tests and plots of liquid-penetration and spray cross-section area are presented. Maximum penetration was found to vary as the square root of the dynamic-pressure ratio and the square root of the total injection nozzle area. Spray cross-section area was linear with maximum penetration. The test results are used to compute injection parameters for the RAM C-III flight injection experiment.</p>			
17. Key Words (Suggested by Author(s)) Liquid injection Flat plate Hemisphere-cone Penetration Hypersonic Mach number Multiple orifices		18. Distribution Statement Unclassified - Unlimited	
19. Security Classif. (of this report) Unclassified	20. Security Classif. (of this page) Unclassified	21. No. of Pages 68	22. Price* \$3.00

MULTIPLE-ORIFICE LIQUID INJECTION
INTO HYPERSONIC AIRSTREAMS AND APPLICATION
TO RAM C-III FLIGHT

By William L. Weaver
Langley Research Center

SUMMARY

Experimental data are presented for the oblique injection of water and three electrophilic liquids (fluorocarbon compounds) through multiple-orifice nozzles from a flat plate and the sides of a hemisphere-cone (0.375 scale of RAM C spacecraft) into hypersonic airstreams. The nozzle patterns included single and multiple orifices, single rows of nozzles, and duplicates of the RAM C-III nozzles. The flat-plate tests were made at Mach 8. Total pressure was varied from 3.45 MN/m^2 to 10.34 MN/m^2 , Reynolds number was varied from 9.84×10^6 per meter to 19.7×10^6 per meter, and liquid injection pressure was varied from 0.69 MN/m^2 to 3.5 MN/m^2 . The hemisphere-cone tests were made at Mach 7.3. Total pressure was varied from 1.38 MN/m^2 to 6.89 MN/m^2 , Reynolds number was varied from 3.54×10^6 per meter to 17.7×10^6 per meter, and liquid-injection pressure was varied from 0.34 MN/m^2 to 4.14 MN/m^2 . Photographs of the tests and plots of liquid-penetration and spray cross-section area are presented. Maximum penetration was found to vary as the square root of the dynamic-pressure ratio and the square root of the total injection nozzle area. Spray cross-section area was linear with maximum penetration. The test results are used to compute injection parameters for the RAM C-III flight injection experiment.

INTRODUCTION

Project RAM (Radio Attenuation Measurements) at the Langley Research Center has, for several years, studied the problem of radio-frequency signal blackout produced by ionization surrounding a spacecraft during high-speed entry into the earth's atmosphere. Four flight experiments, which were flown on Scout vehicles from Wallops Island, Virginia, have been conducted during this program to investigate liquid injection as a technique for reducing radio-signal attenuation caused by this entry plasma. Results from the first three flight experiments are reported in references 1 to 3, and preliminary results from the fourth (RAM C-III) are reported in reference 4.

Most of the liquid injection studies prior to RAM have investigated the case of single-orifice injection into two-dimensional airflow (refs. 5 to 10, for example). The RAM flight experiments have investigated the case of multiple-orifice liquid injection into the flow fields of blunt bodies, and several wind-tunnel injection studies have been conducted to provide the injection data required in the flight-experiment design and in the analyses of the flight data. The studies of references 2 and 11 included tests with scale models of the GT-3 and RAM B-II spacecraft, and the study of reference 12 included tests in which the model and injection nozzles were scaled to the ram C-I flight hardware. Data from reference 12 and from the C-I flight indicated some areas in which changes in the nozzle design could improve injection performance; consequently further studies were carried out prior to the flight of the RAM C-III experiment. The first of these studies (reported in ref. 13) showed an increase in penetration due to jet shielding (first reported in ref. 12) for up to three orifices in a row on a flat plate. Reference 13 showed also that the point of maximum penetration is moved rearward when the orifices are angled downstream from the normal, a fact that led to angling the nozzles downstream for RAM C-III, reducing the possibility of shock disturbance by the jets near the injection site.

In the studies of the current report, water and fluorocarbons were injected from multiple-orifice-nozzle patterns on a flat-plate model and the sides of a hemisphere-cone. The nozzles tested on the hemisphere-cone included duplicates of those flown on RAM C-III, and the data were used in conjunction with flight-measured data to infer flight injection parameters.

Most of the liquid-injection studies continue to investigate the case of single-orifice injection from a flat plate (refs. 14 to 16, for example). In reference 15 liquid penetration for single-orifice injection from a flat plate was correlated by an expression which indicated a Mach number effect; but a Mach number independent parameter can be obtained by transformation that is basically the same as that which correlates the penetration data of references 12 and 13 and this report. The agreement shown in reference 12 between water-spray trajectories measured with single-orifice injection from a hemisphere-cone and trajectories computed by the equations of reference 16 is now believed to be fortuitous.

SYMBOLS

A_j	total jet or nozzle area
A_s	spray cross-section area
a	slope of line for nondimensional penetration
C_j	orifice discharge coefficient (see eq. (1))

D_e	equivalent orifice diameter (see eq. (5))
D_j	measured orifice diameter
d_j	effective orifice diameter, $C_j D_j$
h	altitude
M	Mach number
\dot{m}_j	liquid flow rate (one side only for hemisphere-cone)
\dot{m}_j^*	liquid flux, \dot{m}_j/A_S (one side only for hemisphere-cone)
n	number of orifices (one side only for hemisphere-cone)
p	pressure
q	dynamic pressure
$q_{L,e}$	equivalent local dynamic pressure
\bar{q}	jet-to-free-stream dynamic-pressure ratio, $\frac{\rho_j V_j^2}{\rho_\infty V_\infty^2}$
V	velocity
$V_j' = \frac{V_j}{C_j}$	
X, Y	axes defined in figure 5
X', Y'	axes defined in figure 27
Δy	maximum liquid penetration (defined in fig. 5)
α	injection angle (defined in fig. 5)
ρ	liquid or gas density
γ	specific-heat ratio

Subscripts:

j	liquid or jet
L	local airstream
∞	free stream
fp	flat plate
hc	hemisphere cone
I	line intercept (see eq. (2) and table III)

TEST FACILITIES, APPARATUS, AND METHODS

Wind Tunnels

The flat-plate model tests were conducted in the Langley Mach 8 variable-density tunnel. This is a blowdown tunnel capable of operating at total pressures up to 20.20 MN/m² and total temperatures up to 840^o K. A description of this facility is given in reference 17. In the current tests, the free-stream total pressure was varied between 3.45 MN/m² and 10.34 MN/m², Reynolds number was varied between 9.84×10^6 per meter and 19.7×10^6 per meter, and the temperature was varied between 640^o K and 810^o K.

The hemisphere-cone model tests were conducted in the Ames 3.5-foot hypersonic wind tunnel. This is a variable-density blowdown tunnel capable of operating at nominal Mach numbers of 5, 7, and 10, total pressures up to 13.55 MN/m², and temperatures up to 1170^o K. A brief description of this facility is given in reference 18. The current tests were conducted at a Mach number of 7.3. Free-stream total pressure was varied between 1.38 MN/m² and 6.89 MN/m²; Reynolds number was varied between 3.54×10^6 per meter and 17.7×10^6 per meter; and temperature was constant at 830^o K.

Models and Injection Nozzles

A sketch of the stainless-steel flat-plate model and the nozzle assembly tested in the Langley Mach 8 tunnel is shown in figure 1, and a sketch of the stainless-steel hemisphere-cone model and nozzle-disk assemblies for the Ames tests is shown in figure 2. The nozzle assembly for the flat-plate model was built into the plate and interfaced with the plenum. The assembly was built to receive the same nozzle inserts as those for the hemisphere-cone which are shown in figure 2(b).

The hemisphere-cone model had a 5.715-cm-radius hemisphere nose which faired into the 9° half-angle cone. This is a 0.375-scale model of the RAM C spacecraft and is similar to the test model of reference 12. The wedge fins simulated the external configuration of the electrostatic and fixed bias probes which were used on the spacecraft to measure electron and ion densities. The nozzle disks interfaced with the plenum and were built to receive the nozzle inserts from their bottom sides.

A complete list of the nozzle patterns tested on both models, along with other pertinent information, is given in table I. The number in the open circles denotes the number of orifices in that nozzle, and the solid circles denote plugged nozzles.

Injection Systems and Test Procedures

Injection pressure for the hemisphere-cone tests was provided by a high-pressure gaseous nitrogen source. Pressure was monitored at the regulator and by a transducer in the plenum, and temperature was monitored by a thermocouple in the plenum. For a tunnel test run, a set of injection pressures was preselected and the regulator was set at the first pressure required. After the tunnel reached steady-state operating conditions, the liquid control valve was opened by a remote switch. When steady-state liquid flow was established, photographic equipment was operated, and liquid temperature, pressure, and flow rate were recorded. When all data required had been taken for the first injection pressure, the control valve was closed, the regulator was adjusted to a new pressure, and the liquid-injection procedure was repeated.

The pressure system and instrumentation for the flat-plate tests were basically the same as that for the hemisphere-cone tests. The test procedures were also the same except that only one injection pressure was used during each test run.

Photographic Techniques

In the flat-plate tests scattered-light and schlieren photographs were made of the injection in the vertical plane. A coordinate system for making measurements from the scattered-light photographs was established prior to the tests by photographing a grid card which was placed along the center line perpendicular to the flat plate. The camera was mounted rigidly and was not moved during the tests. The lateral cross section of the spray was recorded by a third camera which was mounted at an angle to the plate. A narrow slit of high-intensity light was used to illuminate the spray cross section. A photograph of a grid card mounted in the proper position and orientation permitted determination of the area of the liquid cross section from the photographs. A schematic of the liquid spray and photographs illustrating the two types of photographs from which measurements were made in the flat-plate tests are shown in figure 3. Further details on the photographic techniques used can be found in reference 13.

In the hemisphere-cone tests scattered-light and schlieren cameras were positioned so that their focal axes were normal to and at the same height as the model center line. The image of the entire model was recorded so that measurements of liquid spray could be scaled directly by the proper model-to-image factors.

Liquids

The four liquids tested are listed along with some of their physical properties in table II. The three fluorocarbon compounds are all electrophilic, which means they have an affinity for the capture of electrons. They are all produced commercially. These are the same four liquids used in the tests of reference 13, and water and the Freon E-3 were the liquids tested in the RAM C-III flight experiment.

DATA REDUCTION

Liquid Velocity

The initial liquid velocity was required in the analysis of the penetration data. Velocity was computed by the following relationship:

$$V_j = C_j \sqrt{\frac{2p_j}{\rho_j}} \quad (1)$$

Using this expression is equivalent to treating the less-than-ideal liquid flow from an orifice as resulting from a reduction in velocity. Some investigators have treated the flow reduction as resulting from a reduction in the cross-section area of the orifice. It will be seen that this is the case for the study of reference 15. The nozzle-discharge coefficients for most of the nozzle patterns tested were determined by calibration prior to the tests. Figure 4 shows plots of the discharge coefficients for several typical nozzle patterns. For the few nozzles for which no calibrations were made, a value of 0.75 was used for the discharge coefficients.

Photographic Measurements

Measurements of maximum liquid (or spray) penetration and measurements of the spray-trajectory coordinates were made from the scattered-light photographs in the flat-plate tests. A grid photograph mentioned earlier was used for these measurements. A grid photograph was also used to measure the spray cross section from the cross-section photographs. The coordinate system and nomenclature used are illustrated in figure 5.

Measurements of maximum liquid penetration were made from the scattered-light photographs in the hemisphere-cone tests. Note that in the sketch of figure 5 maximum penetration measurements are normal to the surface of the cone. In a few cases, no

scattered-light photograph was available, and maximum penetration was measured from the schlieren photographs. Figure 6 shows that maximum-penetration measurements from the scattered-light photographs are, on the average, 16 percent greater than those from the schlieren photographs; so when the schlieren photographs were used, the measured values of penetration were multiplied by the factor 1.16.

RESULTS AND DISCUSSION

Treatment and Presentation of Data

Representative photographs are presented for tests with each nozzle pattern for both models. The penetration data are plotted against \sqrt{q} . In some cases the maximum penetration is nondimensionalized by the total area of the injection nozzles. Lines are faired through all the data; and, whereas the maximum penetration would actually go to zero at $\sqrt{q} = 0$, some faired lines have nonzero intercepts at $\sqrt{q} = 0$. The equations for the lines of nondimensional maximum penetration are given in table III along with other pertinent information. This equation has the form

$$\frac{\Delta y}{\sqrt{A_j}} = a\sqrt{q} + \left(\frac{\Delta y}{\sqrt{A_j}}\right)_I \quad (2)$$

The reference figure refers to the figure where the nondimensional line is shown.

Single-Orifice Data

Tests were run only with water injection from a single 0.0508 cm-diameter orifice for both the flat-plate and hemisphere-cone models. Photographs of these tests are shown in figure 7. Plots of the maximum-water-penetration data are shown in figure 8. The plots include data from the single-orifice investigation of reference 13. The flat-plate data are also used for the more general correlation of maximum penetration for injection from single nozzles; these data are covered in the next section.

In the tests of reference 15, several liquids were injected from single orifices on a flat plate. The penetration y at a distance $x = 150d_j$ downstream from the injection site was found to be correlated by the parameter

$$\frac{yM_\infty}{d_j} \propto \left(\frac{p_j}{p_\infty}\right)^{0.51} \quad (3)$$

The authors of reference 15 showed that this parameter also correlated single-orifice penetration data from other tests at different Mach numbers. They thus concluded that penetration was dependent on Mach number and that this parameter accounted for the

effect. Substituting the relationships

$$p_j = \frac{1}{2} \rho_j (V_j')^2$$

$$p_\infty = \frac{2q_\infty}{\gamma M_\infty^2} = \frac{\rho_\infty V_\infty^2}{\gamma M_\infty^2}$$

into equation (3) and transforming reduces the correlation to approximately

$$\frac{y}{D_j} \propto \sqrt{q} \quad (4)$$

Thus the apparent Mach number effect was primarily due to a change in dynamic pressure with Mach number at a constant value of static pressure. This parameter has the same basic form as that which is used to correlate all the data in the current paper.

The tests of reference 16 were all run with normal and upstream liquid injection; however the authors did not restrict the application of the spray-trajectory equations which they developed to this set of injection angles. Figure 9 shows comparisons of measured spray trajectories with spray trajectories computed by the equations of reference 16. One comparison is for data from the current tests and one is from the data of reference 13. It can be seen that in both cases the equations underpredict the spray penetration even though the basic shape is predicted. It should be noted that the measurements of penetration used in reference 16 to develop these equations were based on spray trajectories which extended, on an average, of only about 5 cm downstream of the injection site. The same is true of the data of reference 15. It can be seen from the photographs (fig. 7) and the trajectory plots (fig. 9) that the spray trajectories are not fully developed at these downstream distances in the current tests. Another possible reason for the disagreement could be the large differences in the dynamic pressures between the current tests and those of reference 16.

Single-Nozzle Data

All of the single-nozzle tests were made with water. Test nozzles for the hemisphere-cone model consisted of one, three, five, or seven orifices of 0.0508 cm diameter. The flat-plate-model nozzles consisted of five or seven orifices of 0.0254 cm diameter and of one, three, five or seven orifices of 0.0508 cm diameter. Photographs of single-nozzle injection tests are presented in figure 10.

Penetration data.- Figure 10(a) shows photographic comparisons of injection with two different orifice diameters in different nozzles. The effect of doubling the orifice

diameter has a significant effect on penetration. Figure 11 shows the maximum penetration data for these tests. These data also help constitute the more general correlation of maximum penetration for single nozzles to be discussed below.

Figures 10(b) and 10(c) show the effect of increasing the number of orifices in a nozzle for the flat-plate tests and the hemisphere-cone tests for 0.0508 cm-diameter orifices. There is a clearly observed effect on penetration for tests with both models when orifices are added to a nozzle. This may not seem to be a surprising result; however multiple-orifice data obtained in reference 2 indicated that penetration was a function of the diameter of one orifice only and did not depend on the number of orifices. The larger spacing between orifices in the tests of reference 2 may have been a factor in the apparent disagreement of that data with the data of this report. The increased penetration due to an increase in orifice number in a nozzle significantly influenced the injection-experiment design for RAM C-III.

The correlation of the nondimensional maximum penetration data for the single nozzles is shown in figure 12. The penetration is seen to be a function of the square root of the total injection nozzle area A_j . Thus the penetration is proportional to an equivalent orifice diameter

$$D_e = \sqrt{n} D_j \quad (5)$$

This is consistent with the data of reference 15 which also shows the penetration from a single orifice to be proportional to the orifice diameter. The flat-plate correlation includes data with the clusters of 0.0254 and 0.0508 cm-diameter orifices.

Spray cross-section data.- Figure 10(d) shows some photographic comparisons of the effects of various factors on the spray cross-section area, and figure 13 shows the correlation of the measured spray cross-section area with the maximum penetration. The plotted cross-section data reflect the effects illustrated in the photographs. The average lateral spreading of the spray is approximately constant with penetration for each of the three sets of data plotted (see also the dynamic-pressure-ratio effect photographs of fig. 10(d)) and increases with injection nozzle area to that of a cluster of three 0.0508 cm-diameter orifices.

Data With Single Rows of Nozzles

The flat-plate model tests included several different combinations of in-line nozzles. (See table I.) The hemisphere-cone model tests were all made with water injection from nozzles of five orifices each with all orifices 0.0508 cm diameter. Figure 14 shows photographs of the in-line nozzle tests. It can be seen in figure 2(b) that there is a difference in spacing of the nozzles between disks 1 and 2. A comparison of injection from three

nozzles using the two disks is shown in figure 14(a). It was concluded that this difference in nozzle spacing does not have a significant effect on penetration.

Penetration data.- An increase in penetration for downstream nozzles can be seen in most of the photographs of figures 14(a) to 14(d). This increase in penetration due to jet shielding was first reported in reference 12, and it was shown in reference 13 to extend two orifices downstream from the first orifice for four different combinations of injection angles. Reference 15, however, concluded that normal injection from two in-line orifices produced the same penetration as that of a single orifice.

The correlations of nondimensional maximum liquid penetration are presented in figure 15. The water-injection data with the flat plate (excluding the row of three single orifices) are in very good agreement with the correlation of the single-nozzle water-injection data of figure 12(a). The penetration data for the Freon E-3 injection is difficult to interpret, and extrapolation of the Freon E-3 penetration data to nozzles of larger orifices and/or to other classes of nozzles should be made with caution.

The penetration correlation for water injection from the hemisphere-cone is in fair agreement with the correlation obtained for single nozzles. (See fig. 12(b).) The equations representing the correlation lines are summarized in table III.

Spray cross-section data.- Some photographs of the cross sections of the liquid spray for both water and Freon E-3 are shown in figure 14(e) and figure 14(f), respectively. Plots of A_S versus Δy are shown in figure 16. The solid triangles represent penetration heights taken from the cross-section photographs and are not points of maximum penetration. The data indicate that spray cross-section area is approximately linear with maximum penetration. The extrapolated lines which fit these data however have nonzero values of penetration at $A_S = 0$, and thus extrapolation of the data should be made with caution.

Data With RAM C-III Nozzles

Figure 17 shows photographic comparisons of the injection tests with the four RAM C-III nozzles at one test condition. The low-flow water and low-flow Freon E-3 nozzles both have about the same penetration, and the high-flow water nozzle is seen to have greater penetration than the high-flow Freon E-3 nozzle. An interesting point is the apparent thinning out of the Freon E-3 in the high-flow photograph and its near disappearance in the low-flow photograph. Shock interaction between the main bowshock and that produced by the water can be seen in the high-flow water photograph. The maximum penetration data for these nozzle tests are shown in figure 18.

Data With Nozzle Patterns 1 to 4 for Hemisphere-Cone Tests

Figure 19 shows photographs of injection tests with nozzle patterns 1 to 4, and figure 20 presents maximum-penetration data showing the effects of several factors on penetration for nozzle patterns 1 and 2.

In figure 19(a) photographic comparisons of injection with different liquids are presented. Freon E-3 is seen to penetrate about the same as FC-43 at the same test conditions, and water is seen to penetrate a greater distance than Freon E-3. Figures 20(a) and 20(b) show that the maximum penetration of water is greater than that of the fluorocarbons for two different orifice diameters in nozzle pattern 1.

The photographs of figure 19(b) show the effect of orifice diameter for injection of water and fluorocarbons from nozzle pattern 1 and for injection of water from nozzle pattern 2. The difference in maximum penetration due to orifice diameter can be seen for three different cases in figures 20(c), 20(d), and 20(e).

The photographs of figure 19(c) show the effects of adding orifices to nozzles for two different cases. Figures 20(f) and 20(g) show the increase in penetration due to increasing the number of orifices in each nozzle for two different orifice diameters.

Comparison of Flat-Plate Data With Hemisphere-Cone Data

The schlieren photographs of injection from the flat plate generally indicate an unsteady flow pattern once the liquid has begun to break up. Figure 10(b) demonstrates this effect quite clearly. The schlieren photographs of reference 14 also show this unsteady condition in the flow pattern. The schlieren photographs of injection with the hemisphere-cone indicate a more stable flow pattern (see fig. 10(c), for example); this may be due to less resolution, however, since the photographs for the hemisphere-cone nozzles cover a much greater portion of the spray trajectories. Another interesting observation is that in a few cases the scattered-light photographs of injection from the hemisphere-cone indicate that very little liquid is present near the surface of the model just aft of the injection site. This point is demonstrated in the photographs of figure 7(b) and, to a lesser degree, in those of figure 19(b); whereas, the scattered-light photographs of injection from the flat plate show (in almost all cases) that liquid exists on the model surface.

Comparison of maximum penetration between the flat-plate tests and the hemisphere-cone tests can be seen in figure 8. Unfortunately all the data for the flat-plate tests were for values of penetration above 3 cm; whereas the hemisphere-cone data extends from about 2 cm to about 4 cm. Comparisons of the nondimensionalized penetration between

the flat-plate and hemisphere-cone tests can be seen in figure 12 (single nozzles) and in figure 15 (rows of in-line nozzles). The equations of the lines representing these data plots are given in table III. The intercepts of these lines are all zero except for the line which represents the data for the single nozzles on a flat plate. This intercept is -2.5 (see table III).

From table III the line-slope ratio for single nozzles is

$$\frac{a_{fp}}{a_{hc}} = 1.39 \quad (6)$$

and the line-slope ratio for in-line nozzles is

$$\frac{a_{fp}}{a_{hc}} = 1.47 \quad (7)$$

which gives an average line-slope ratio as follows:

$$\frac{a_{fp}}{a_{hc}} = 1.43 \approx \sqrt{2} \quad (8)$$

Equation (8) states that the equivalent dynamic pressure influencing penetration in the flow field of the hemisphere-cone is about twice the pressure for the flat plate at the same free-stream conditions. Thus, for comparison on the basis of \sqrt{q} , the following relationships can be used:

$$(q_{L,e})_{fp} = q_L = q_\infty \quad (9)$$

$$(q_{L,e})_{hc} \approx 2q_\infty \quad (10)$$

Note that $(q_{L,e})_{hc}$ is not the actual local dynamic pressure at any point in the flow field, but is only an equivalent value. The local dynamic pressure as used in reference 12 was the actual value at the injection site and was approximately equal to one-half the free-stream value. It is concluded that the extrapolation of liquid-penetration data to cases of different geometry or flow conditions requires a knowledge of the relation between the flow condition for the two test cases.

COMPUTATIONS OF RAM C-III FLIGHT INJECTION PARAMETERS

The RAM C-III flight experiment was launched from Wallops Island on a four-stage Scout rocket September 30, 1970. A photograph of the rocket and the spacecraft is shown in figure 21, along with a sketch of the spacecraft (15.24 cm-radius hemisphere faired

with 9° cone) and its final stage motor. The spacecraft was boosted to an apogee of 230 km and the final stage motor accelerated the spacecraft to a speed of 7.3 km/sec at an altitude of 137 km. One of the main objectives of the experiment was to compare the effectiveness of an electrophilic liquid with that of water in alleviating radio blackout. Water and the fluorocarbon compound (Freon E-3) were each injected separately through two different nozzles located just aft of the hemisphere-cone junction over an altitude range from 84.8 km to 37.5 km. A more detailed description of the injection experiment is given in reference 4, and data from the experiment are presented. In the current paper the results from the liquid-injection tests reported in earlier sections are used to compute some of the important injection parameters for the RAM C-III flight experiment.

Liquid-Injection Velocity and Flow Rate

The liquid-injection pressure which was measured in flight is shown in figure 22, and these values were used to compute the liquid-injection velocity by equation (1) at the beginning of each injection pulse. The computed velocity is shown in figure 23, along with an illustration of an injection cycle. The flight nozzle discharge coefficients are shown in figure 24. The difference in velocity between the two liquids at about the same injection pressure is due primarily to the difference in densities of the two liquids. (See table II.)

The liquid-flow rates were measured in flight, and the measured values are compared with computed values at the beginning of each injection pulse in figure 25. The flow rates were computed by the relation

$$\dot{m}_j = \rho_j V_j A_j \quad (11)$$

It can be seen that the measured and computed flow rates are in good agreement, except that the measured flow rates from the high-flow Freon E-3 nozzle are about 10 percent lower than the computed rates.

Nozzle Patterns

The flight nozzle patterns were nearly the same as for the test RAM C-III nozzle patterns in the number of nozzles, orifice diameter and number of orifices per nozzle, and the injection angle ($\alpha = 51^\circ$). Figure 26 compares the nozzle spacing for the test and flight nozzle patterns. It can be seen that the largest difference is for the high-flow-water nozzle pattern. It was shown previously in the section on in-line nozzles that the difference in spacing between nozzles on disks 1 and 2 did not have a significant effect on penetration. Jet shielding is the predominant factor in penetration with the in-line nozzles, and it is assumed that the differences in spacing between nozzles for the RAM C-III test and flight nozzle patterns was insignificant.

Local Dynamic Pressure

A comparison of theoretically determined local dynamic pressure adjacent to the injection nozzles was made between the hemisphere-cone test model and the flight spacecraft. A typical comparison is shown in figure 27. Lines of constant dynamic pressure are plotted in the flow field adjacent to the injection nozzles at similar values of free-stream dynamic pressure. This comparison suggests that the injected liquid in flight will traverse a dynamic-pressure flow regime similar to that in the flow field of the test model at the same free-stream dynamic pressure. Thus it was assumed that the penetration data obtained in the hemisphere-cone tests with the RAM C-III nozzles could be extrapolated directly to flight at all altitudes on the basis of \sqrt{q} .

Liquid Penetration and Flow Flux

The entry altitude and velocity of the RAM C-III spacecraft which covers the period of liquid injection are shown in figure 28. Values from these curves were used to compute the free-stream dynamic pressure by the equation

$$q_{\infty} = \frac{1}{2} \rho_{\infty} V_{\infty}^2 \quad (12)$$

where the density has been corrected for the temperature measured the day of the entry flight.

Values of \bar{q} were computed at the beginning of each injection pulse using the values of q_{∞} computed by equation (12) and the values of V_j from figure 23. A plot of $\sqrt{\bar{q}}$ is shown in figure 29. These values are used with figure 18 (penetration data for RAM C-III nozzles) to determine values of maximum liquid penetration during flight.

The liquid flow flux, which is a measure of the amount of liquid flowing through a unit area in the flow field in unit time, is computed by the following expression:

$$\dot{m}_j^* = \frac{\dot{m}_j}{A_S} \quad (13)$$

The computed values of \dot{m}_j given in figure 25 were used in this computation. No data were available on the spray cross-section area for injection from a hemisphere-cone, and the values required for this parameter were taken from the flat-plate test data. Figures 13 and 16 were used to infer A_S as a function of Δy . The work of reference 19 has indicated that there may be diffusion of the fluorocarbon in the blunt-body flow field, and the inferred values of the Freon E-3 flow flux may be conservative. A composite plot of the inferred liquid penetration, flow rate, and flow flux is given in figure 30.

The penetration is seen to rise gradually to a peak value at an altitude of about 55 km and then to decrease because of a rapid increase in free-stream dynamic pressure. The liquid-flow rates from all nozzles are seen to increase during most of the injection period,

but the increase is very slight during the last three injection cycles. The liquid flux, however, is seen to increase most rapidly during the last few cycles, due primarily to the decrease in spray cross-section area which results from the decrease in liquid penetration.

CONCLUDING REMARKS

Experimental data are presented for the oblique injection of water and three electrophilic liquids through multiple-orifice nozzles from a flat plate and the sides of a hemisphere-cone (0.375 scale of RAM C spacecraft) into hypersonic airstreams. Photographs of the tests and correlation plots of the maximum liquid penetration and the liquid-spray cross sections are presented. The data reflect the following conclusions:

- (1) Maximum liquid penetration increases as the square root of the jet-to-free-stream dynamic-pressure ratio for all nozzles tested.
- (2) Penetration obtained with single-orifice water injection from the flat plate was underpredicted by the correlations of earlier investigations.
- (3) Maximum liquid penetration increases with the number of orifices in a nozzle.
- (4) Maximum penetration is increased due to jet shielding for at least four nozzles downstream from the first nozzle.
- (5) Penetration for single nozzles and single rows of nozzles increases as the square root of the total injection nozzle area.
- (6) Water penetrates farther than does fluorocarbon.
- (7) Liquid-spray cross-section area for injection from the flat plate increases linearly with maximum penetration.
- (8) Comparisons of maximum penetration between the flat-plate and hemisphere-cone tests indicate that the effective airstream dynamic pressure influencing penetration in the hemisphere-cone flow field was about twice that of the free stream.

The test results were used to compute post-flight injection parameters for the RAM C-III flight experiment. The following results were obtained:

- (1) The similarity of the test-model flow field with that of the spacecraft flow field in flight indicates that penetration can be predicted on the basis of in-flight jet-to-free-stream dynamic-pressure ratio.
- (2) Penetration was about the same for the two low-flow water nozzles but it was greater for the high-flow water nozzle than for the high-flow Freon E-3 nozzle. The greatest penetration occurred at about 55 km altitude and then decreased because of the rapid increase in the flight dynamic pressure.

(3) Flow rates generally increased during injection, but the increase was small after 50 km because of the tapering off of injection pressure.

(4) Liquid fluxes increased continually during injection, but the greatest increase was near the end of injection when the spray cross section was decreasing rapidly.

Langley Research Center,
National Aeronautics and Space Administration,
Hampton, Va., December 23, 1971.

REFERENCES

1. Cuddihy, William F.; Beckwith, Ivan E.; and Schroeder, Lyle C. (With appendix A by Ivan E. Beckwith, Dennis M. Bushnell, and James L. Hunt; appendix B by Ivan E. Beckwith and Sadie P. Livingston; and appendix C by Ivan E. Beckwith): Flight Test and Analysis of a Method for Reducing Ratio Attenuation During Hypersonic Flight. NASA TM X-1331, 1967.
2. Beckwith, Ivan E.; Bushnell, Dennis M.; and Huffman, Jarrett K.: Investigation of Water Injection on Models of Gemini Vehicle and Resulting Predictions for GT-3 Reentry Communications Experiment. NASA TM X-1200, 1966.
3. Akey, Norman D.; and Cross, Aubrey E. (With appendix A by Thomas G. Campbell; appendix B by Fred B. Beck; and appendix C by W. Linwood Jones, Jr.): Radio Blackout Alleviation and Plasma Diagnostic Results From a 25,000 Foot Per Second Blunt-Body Reentry. NASA TN D-5615, 1970.
4. Schroeder, Lyle C.: Flight Measurements at 25 000 Feet Per Second of Blackout Alleviation by Water and Electrophilic Injection. The Entry Plasma Sheath and Its Effects on Space Vehicle Electromagnetic Systems, Vol. II, NASA SP-253, 1971, pp. 77-100.
5. Ingebo, Robert D.; and Foster, Hampton H.: Drop-Size Distribution for Crosscurrent Breakup of Liquid Jets in Airstreams. NACA TN 4087, 1957.
6. Weiss, Malcolm A.; and Worsham, Charles H.: Atomization in High Velocity Air-streams. ARS J., vol. 29, no. 4, Apr. 1959, pp. 252-259.
7. Bitron, Moshe D.: Atomization of Liquids by Supersonic Air Jets. Ind. Eng. Chem., vol. 47, no. 1, 1955, pp. 23-28.
8. Chelko, Louis J.: Penetration of Liquid Jets Into a High-Velocity Air Stream. NACA RM E50F21, 1950.
9. Ingebo, Robert D.: Study of Pressure Effects on Vaporization Rate of Drops in Gas Streams. NACA TN 2850, 1953.
10. Shapiro, A. H.; Wadleigh, K. R.; Gavril, B. D.; and Fowle, A. A.: The Aerothermopressor - A Device for Improving the Performance of a Gas-Turbine Power Plant. Trans. ASME, vol. 78, no. 3, Apr. 1956, pp. 617-653.
11. Beckwith, Ivan E.; and Huffman, Jarrett K.: Injection and Distribution of Liquids in the Flow Fields of Blunt Shapes at Hypersonic Speeds. NASA TM X-989, 1964.
12. Weaver, William L.; and Hinson, William F.: Water Injection From a 90° Hemisphere-Cone Into a Hypersonic Airstream. NASA TN D-5739, 1970.

13. Hinson, William F.; Gooderum, Paul B.; and Bushnell, Dennis M.: Experimental Investigation of Multiple-Jet Liquid Injection Into Hypersonic Flow. NASA TN D-5861, 1970.
14. Hill, D. E.: Penetration of a Liquid Jet Injected Into a Gas Stream. Rep. SM-47782 (Rev.), Douglas Missile & Space Systems Div., Oct. 1965.
15. Kolpin, M. A.; Horn, K. P.; and Reichenback, R. E.: Study of Penetration of a Liquid Injectant Into a Supersonic Flow. AIAA J., vol. 6, no. 5, May 1968, pp. 853-858.
16. Catton, I.; Hill, D. E.; and McRae, R. P.: Study of Liquid Jet Penetration in a Hypersonic Stream. AIAA J., vol. 6, no. 11, Nov. 1968, pp. 2084-2089.
17. Schaefer, William T., Jr.: Characteristics of Major Active Wind Tunnels at the Langley Research Center. NASA TM X-1130, 1965.
18. Hopkins, Edward J.; Rubesin, Morris W.; Inouye, Mamoru; Keener, Earl R.; Mateer, George C.; and Polek, Thomas E.: Summary and Correlation of Skin Friction and Heat-Transfer Data for a Hypersonic Turbulent Boundary Layer on Simple Shapes. NASA TN D-5089, 1969.
19. Kurzius, Shelby C.; and Raab, Fredrik H.: Vaporization and Decomposition Kinetics of Candidate Re-Entry Blackout Suppressants in Low Pressure Flames. NASA CR-1330, 1969.

TABLE I.- TEST NOZZLES AND PERTINENT INFORMATION

Flat-plate model

Nozzle patterns (a)	D _j , cm	Liquid tested
Single orifice	0.0508	Water
Single nozzles of 5 or 7 orifices	0.0254	Water
Single nozzles of 1, 3, 5, or 7 orifices	0.0508	Water
Single rows of 2, 4, or 6 nozzles (5 orifices per nozzle)	0.0508	Water
⑦ ⑦ ⑤ ● ● ●	0.0508	Water
⑦ ⑦ ⑤ ⑤ ③ ③	0.0508	Water
① ① ① ● ● ●	0.0508	Water
① ① ① ① ① ①	0.0254	Fluorocarbon
⑤ ● ⑤ ● ● ⑦	0.0254	Fluorocarbon
⑤ ● ● ⑤ ● ⑦	0.0254	Fluorocarbon
⑤ ● ⑤ ⑤ ● ⑤	0.0254	Fluorocarbon
⑤ ● ⑤ ● ● ⑤	0.0508	Fluorocarbon

^aNumber in circle denotes number of orifices in nozzle.
Solid circle denotes nozzle is plugged.

Hemisphere-cone model

Nozzle patterns (a)	Disk	D _j , cm	Liquid tested
Single orifice	1	0.0508	Water
Single nozzles of 1, 3, 5 or 7 orifices	1	0.0508	Water
Single rows of 1, 2, or 3 nozzles (5 orifices per nozzle)	1	0.0508	Water
Single rows of 4 or 5 nozzles (5 orifices per nozzle)	2	0.0508	Water
RAM C-III (low flow) ⑤ ● ●	1	0.0508	Water
RAM C-III (high flow) ⑤ ⑤ ⑤ ⑤ ●	2	0.0508	Water
RAM C-III (low flow) ① ③ ●	1	0.0508	Fluorocarbon
RAM C-III (high flow) ③ ⑤ ⑦	1	0.0508	Fluorocarbon
Nozzle pattern 1: ① ① ③ ① ① ③ ① ① ③	1	0.0254, 0.0508	Water, Fluorocarbon
Nozzle pattern 2: ⑤ ⑤ ⑦ ⑤ ⑤ ⑦ ⑤ ⑤ ⑦	1	0.0254, 0.0508	Water
Nozzle pattern 3: ① ① ● ● ● ● ① ① ●	2	0.0508	Water, Fluorocarbon
Nozzle pattern 4: ⑤ ⑤ ● ● ● ● ⑤ ⑤ ●	1	0.0508	Water

^aNumber in circle denotes number of orifices in nozzle. Solid circle denotes nozzle is plugged.

TABLE II.- LIQUID PROPERTIES AT 298° K

Identification	Formula	Density, kg/m ³	Vapor pressure, N/m ²	Viscosity, cP	Surface tension (in air), N/m	Heat of vaporization, kJ/kg	Relative atomized mean droplet size	Relative evaporative lifetime of atomized mean droplet size
Water ^a	H ₂ O	997	3173	0.894	0.0720	2258.28	1	1
Freon E-3 ^a	F(C ₃ F ₆ O) ₃ CFHCF ₃	1720	320	2.2	.0142	60.64	---	----
FC-43	(C ₄ F ₉) ₃ N	1880	40	4.9	.0160	69.84	.45	.026
FC-75	C ₈ F ₁₈	1770	4000	1.45	.0148	88.24	.45	.031

^aUsed in RAM C-III flight experiment.

TABLE III.- EQUATIONS FOR LINES OF NONDIMENSIONAL MAXIMUM PENETRATION

$$\left[\frac{\Delta y}{\sqrt{A_j}} = a\sqrt{q} + \left(\frac{\Delta y}{\sqrt{A_j}} \right)_I; \left(\frac{\Delta y}{\sqrt{A_j}} \right)_I = \text{Intercept at } \sqrt{q} = 0 \right]$$

Model	Nozzle patterns	Reference figure	Liquid	D _j , cm	a	$\left(\frac{\Delta y}{\sqrt{A_j}} \right)_I$
Flat plate	Single nozzles of 1, 3, 5, or 7	12(a)	Water	0.0254, 0.0508	13.2	-2.5
Hemisphere-cone	Single nozzles of 3, 5, or 7	12(b)	Water	.0508	9.5	0
Flat plate	In-line nozzles	15(a)	Water	.0508	13.1	0
Flat plate	① ① ① ● ● ●	15(a)	Water	.0508	14.9	7.5
Flat plate	In-line nozzles	15(a)	Fluorocarbon	.0254	5.5	27.5
Hemisphere-cone	In-line nozzles	15(b)	Water	.0508	8.9	0

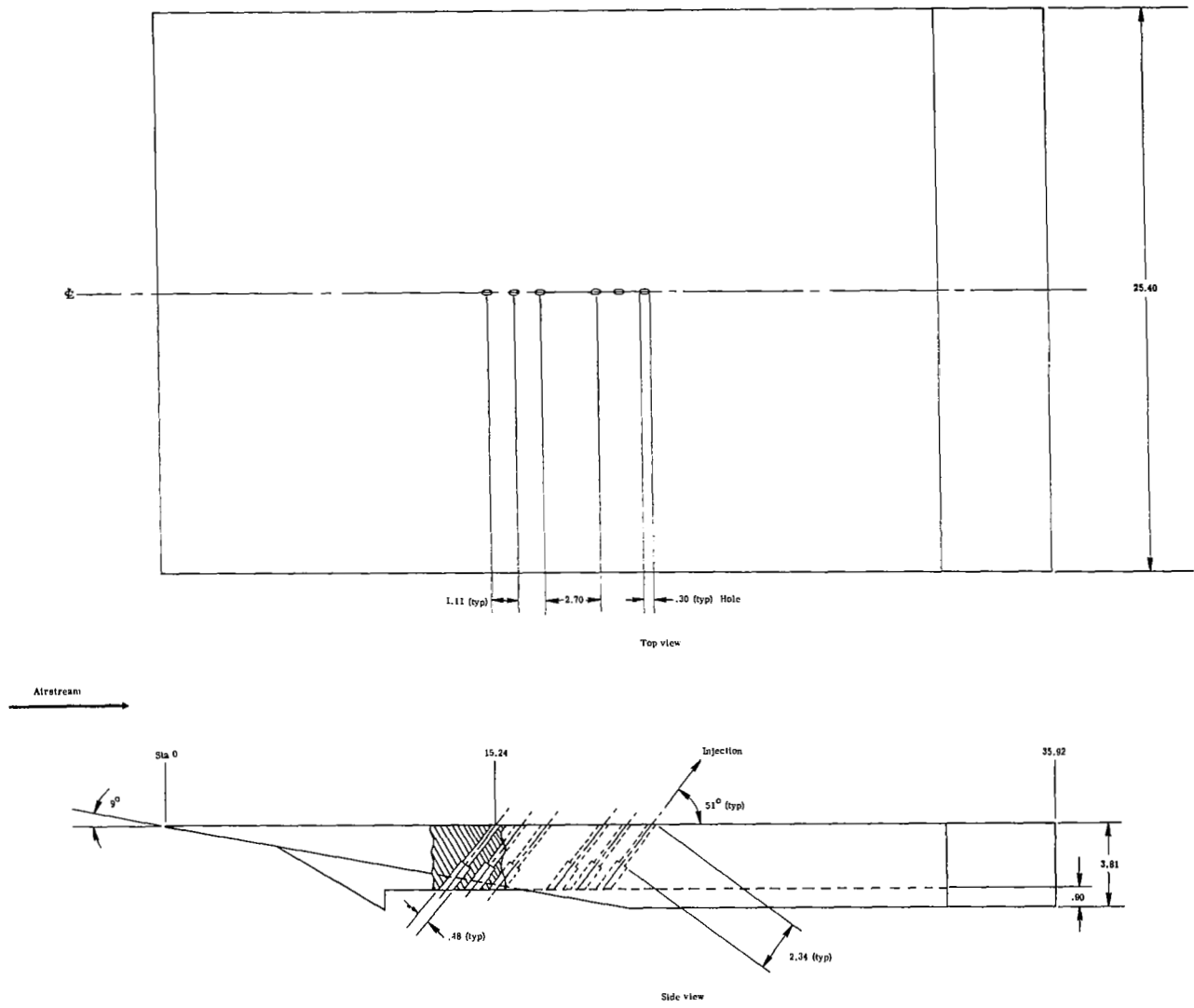
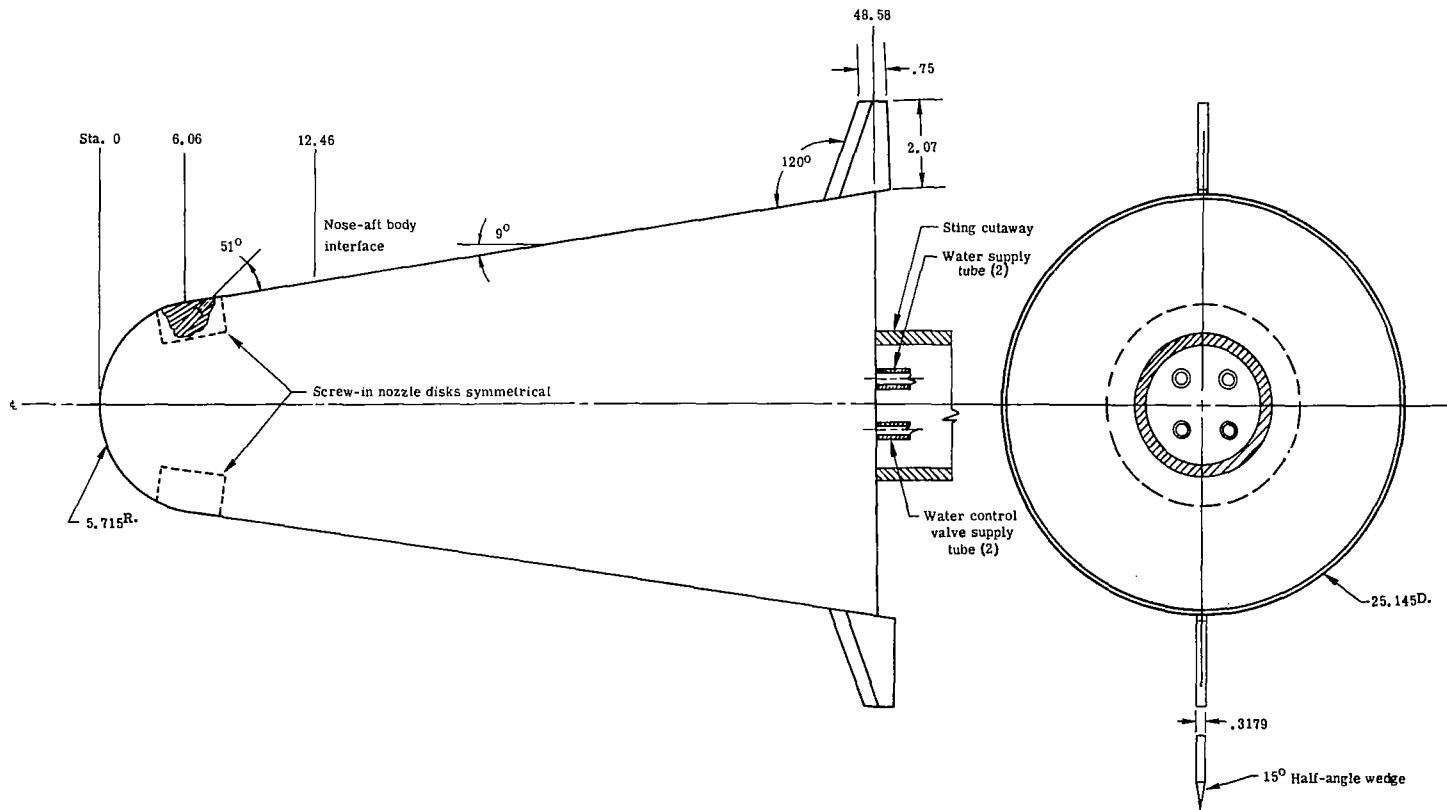
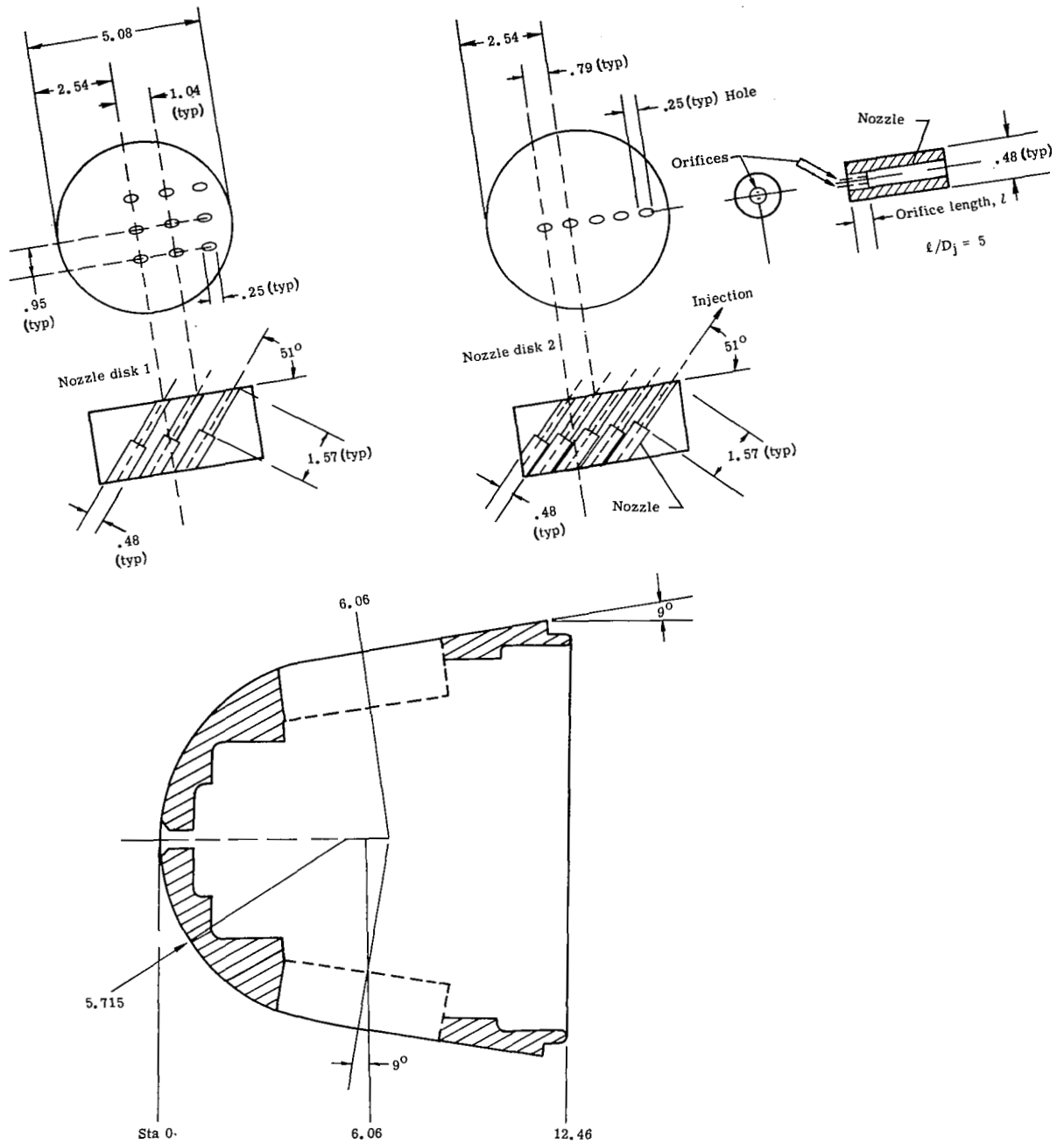


Figure 1.- Flat-plate test model. (All dimensions in cm.)



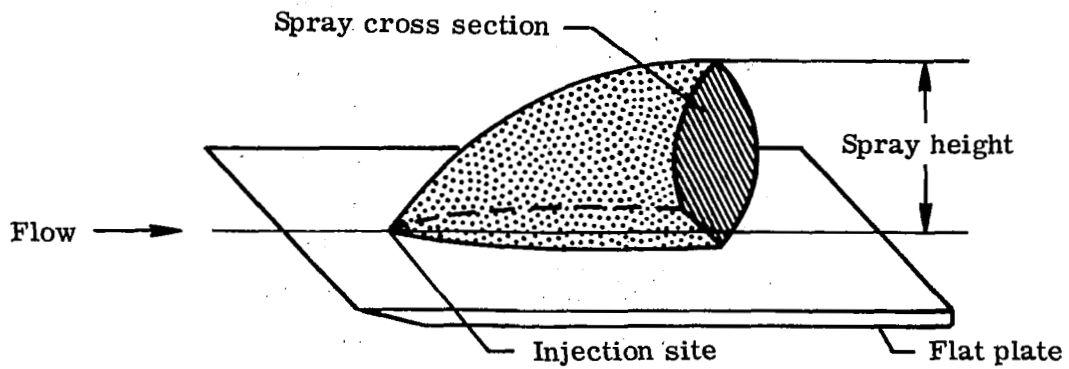
(a) Test model.

Figure 2.- Hemisphere-cone test model and nozzle-disk assemblies. (All dimensions in cm.)

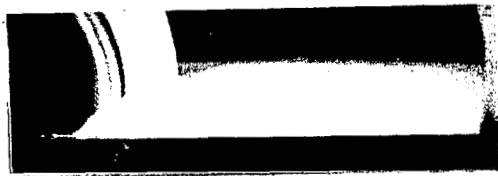


(b) Nozzle-disk assemblies.

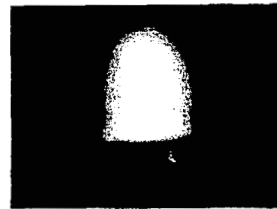
Figure 2.- Concluded.



(a) Schematic of spray.



Scattered light



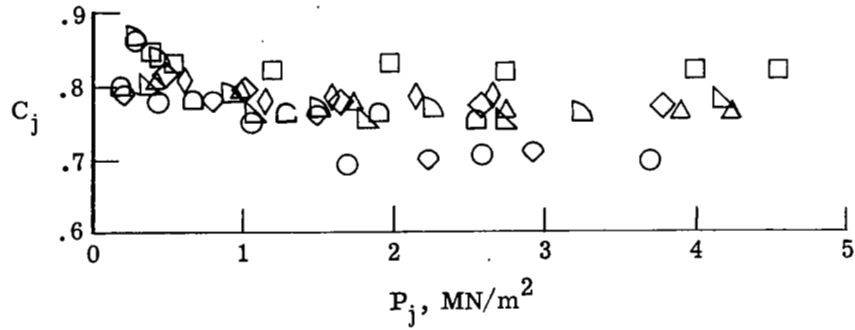
Cross section

L-71-7154

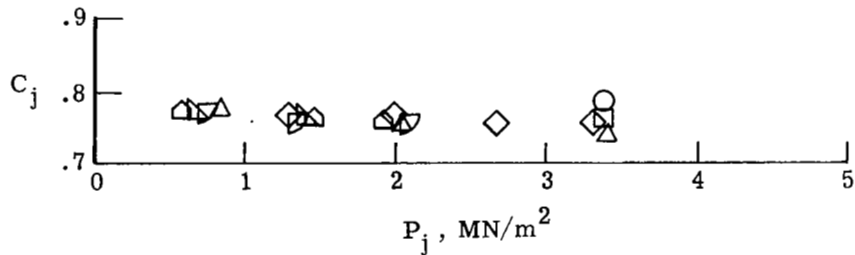
(b) Spray photographs.

Figure 3.- Illustrations of photographic techniques used in flat-plate tests.

Symbol	Nozzle	Liquid
○	①	Water
□	③	Water
◇	⑤	Water
△	⑦	Water
▵	⑤ ⑤	Water
▹	⑤ ⑤ ⑤	Water
◐	RAM C-III Low flow	Fluorocarbon
◑	⑤ ⑤ ⑤ ⑤	Water
◒	⑤ ⑤ ⑤ ⑤ ⑤ ⑤	Water
◓	RAM C-III High flow	Fluorocarbon
◔	Pattern 1	Fluorocarbon

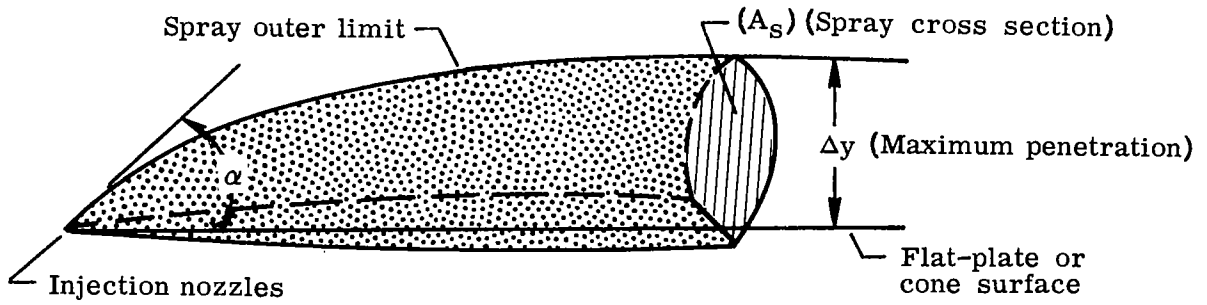


(a) Hemisphere-cone model.

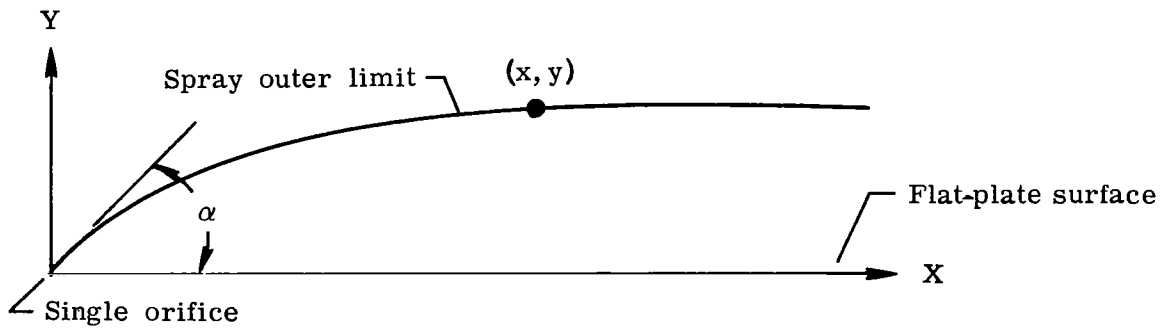


(b) Flat-plate model.

Figure 4.- Nozzle discharge coefficients. $D_j = 0.0508$ cm.



(a) Maximum penetration and spray cross section.



(b) Spray coordinates for single-orifice injection.

Figure 5.- Coordinates and nomenclature.

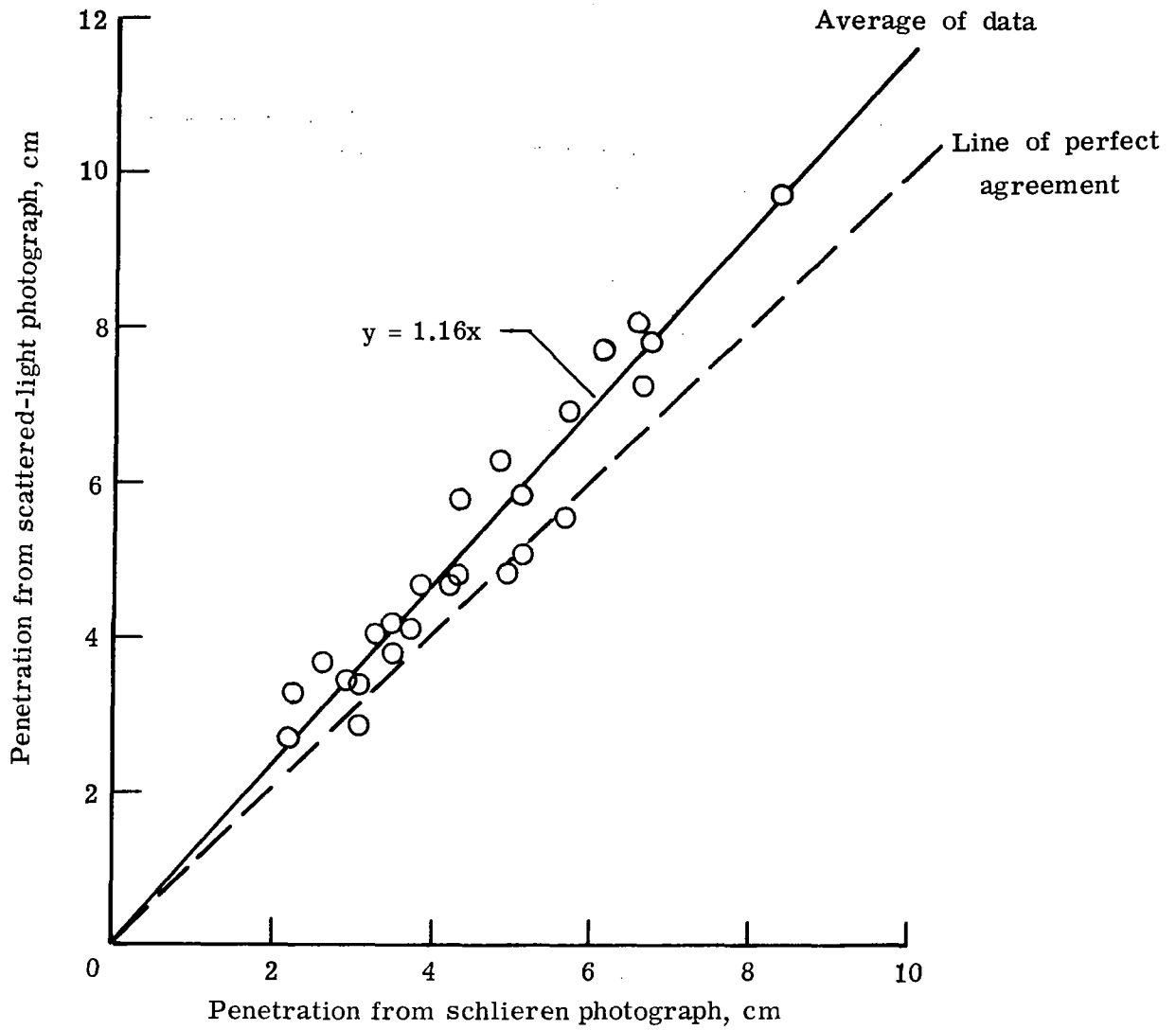
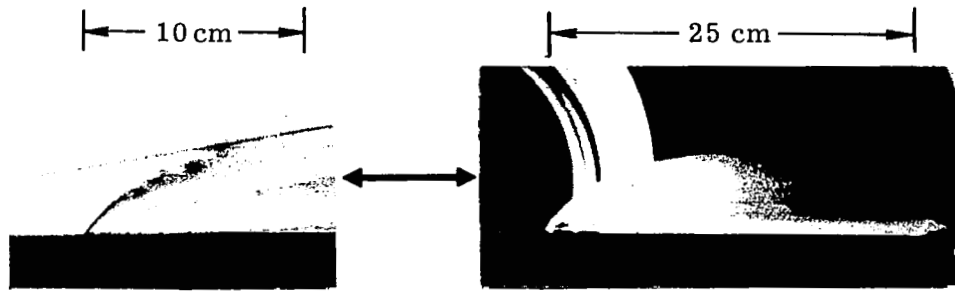
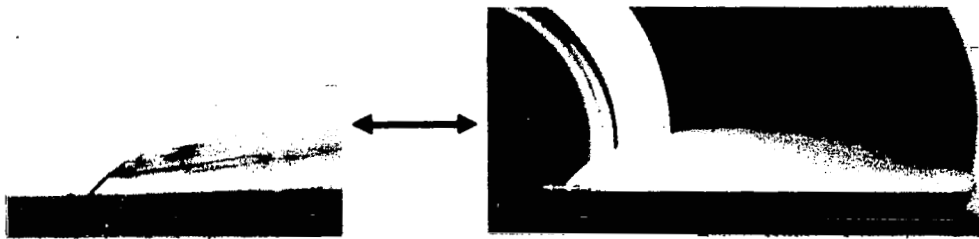


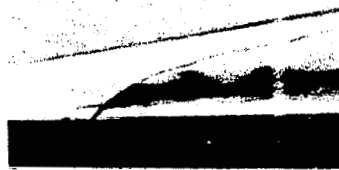
Figure 6.- Comparison of maximum penetration determined from two types of photographs in hemisphere-cone tests.



$$q_{\infty} = 15.8 \text{ kN/m}^2; \bar{q} = 128$$



$$q_{\infty} = 31.6 \text{ kN/m}^2; \bar{q} = 62$$

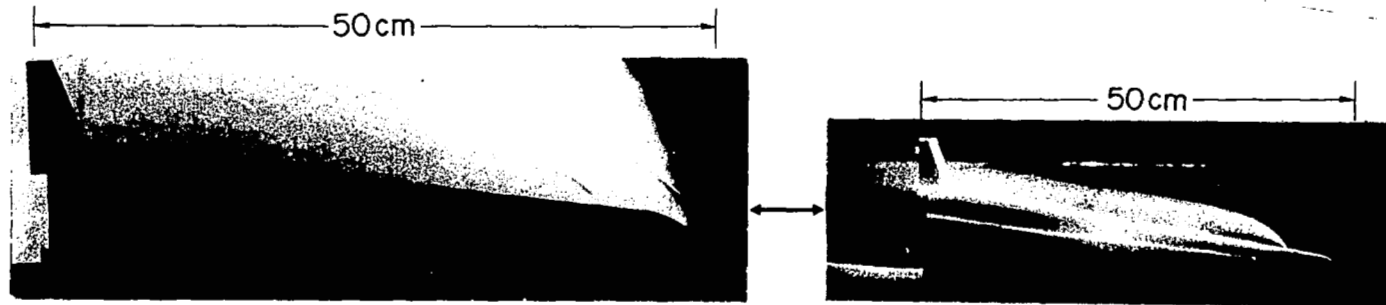


$$q_{\infty} = 47.4 \text{ kN/m}^2; \bar{q} = 44$$

L-71-7155

(a) Side view; flat plate.

Figure 7.- Photographs of water injection with single orifice.



$$q_{\infty} = 22.8 \text{ kN/m}^2; \bar{q} = 30.5$$

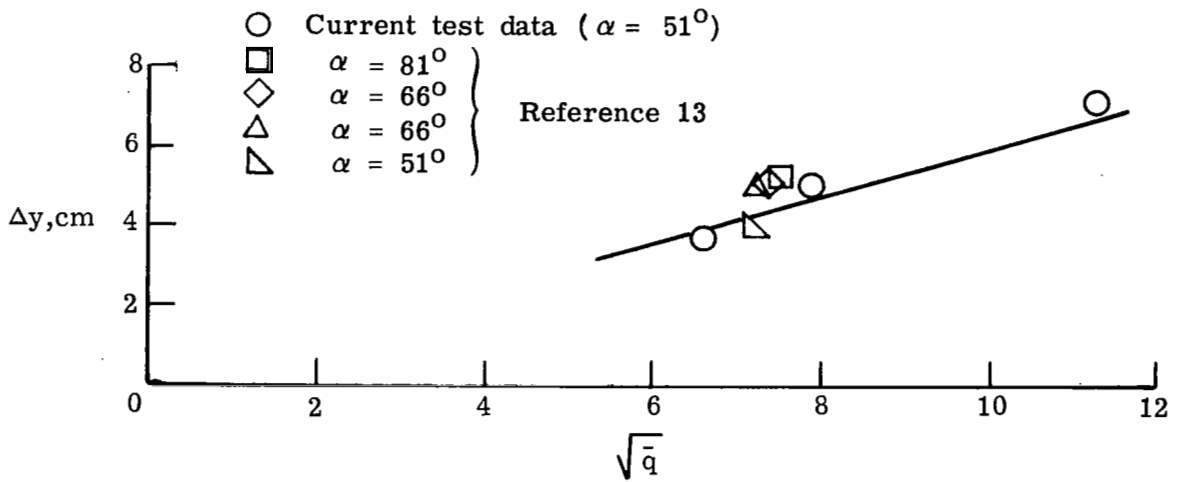


$$q_{\infty} = 43.4 \text{ kN/m}^2; \bar{q} = 83.0$$

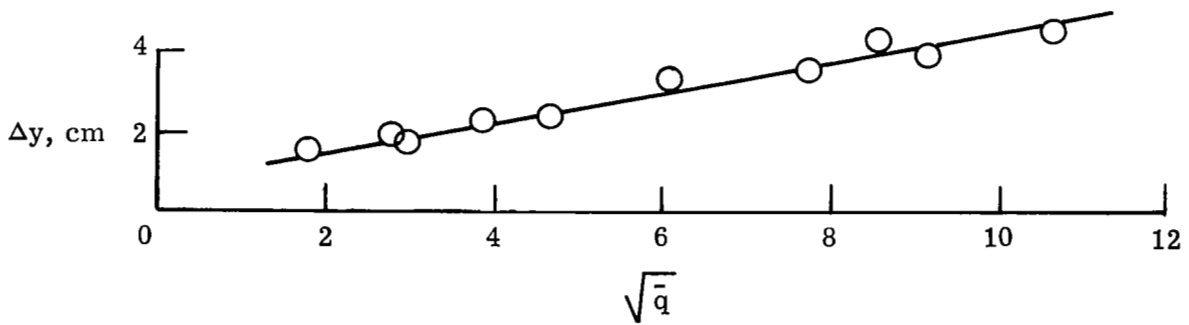
L-71-7156

(b) Side view; hemisphere-cone.

Figure 7.- Concluded.

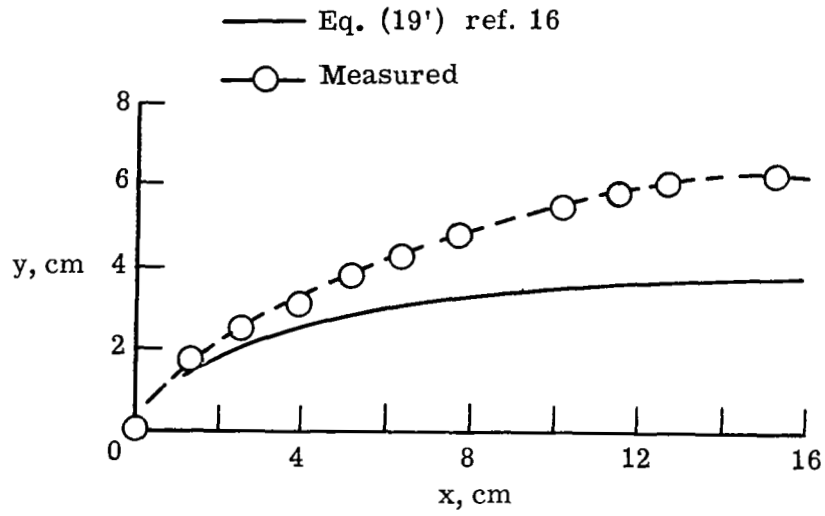


(a) Flat plate.

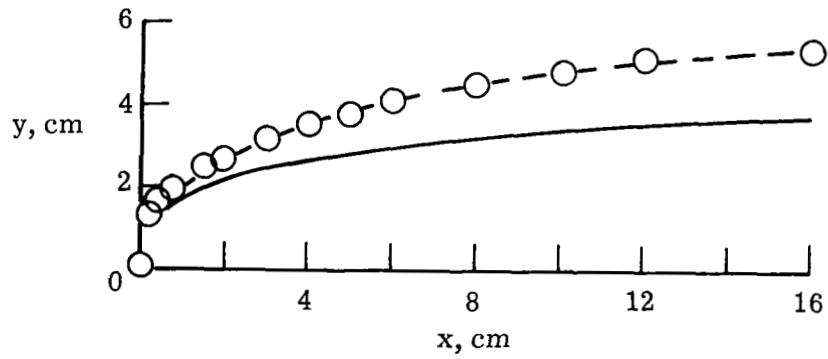


(b) Hemisphere-cone.

Figure 8.- Maximum water penetration with single-orifice injection.

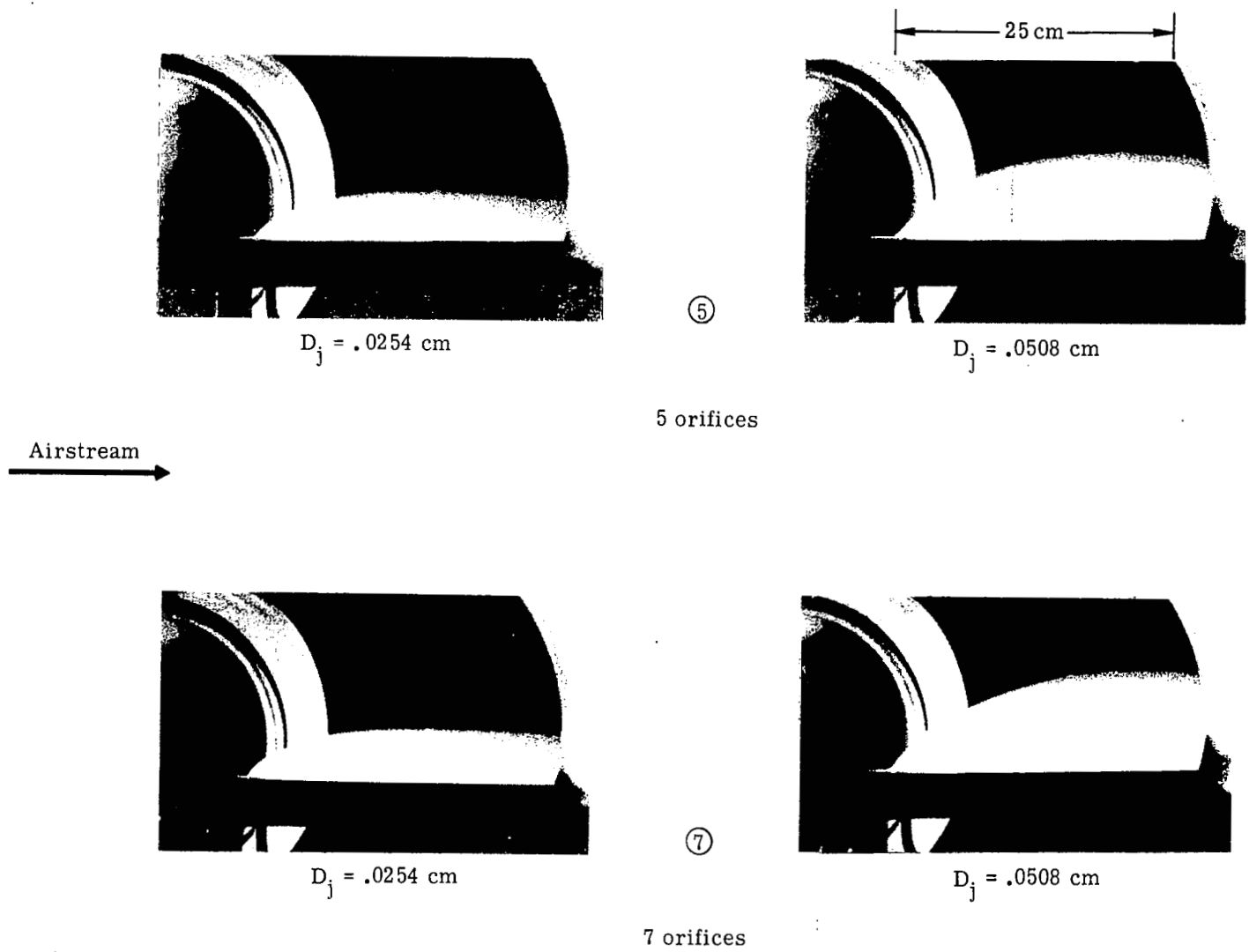


(a) Current data; $\bar{q} = 128$; $\alpha = 51^\circ$.



(b) Data of reference 13; $\bar{q} = 50$; $\alpha = 81^\circ$.

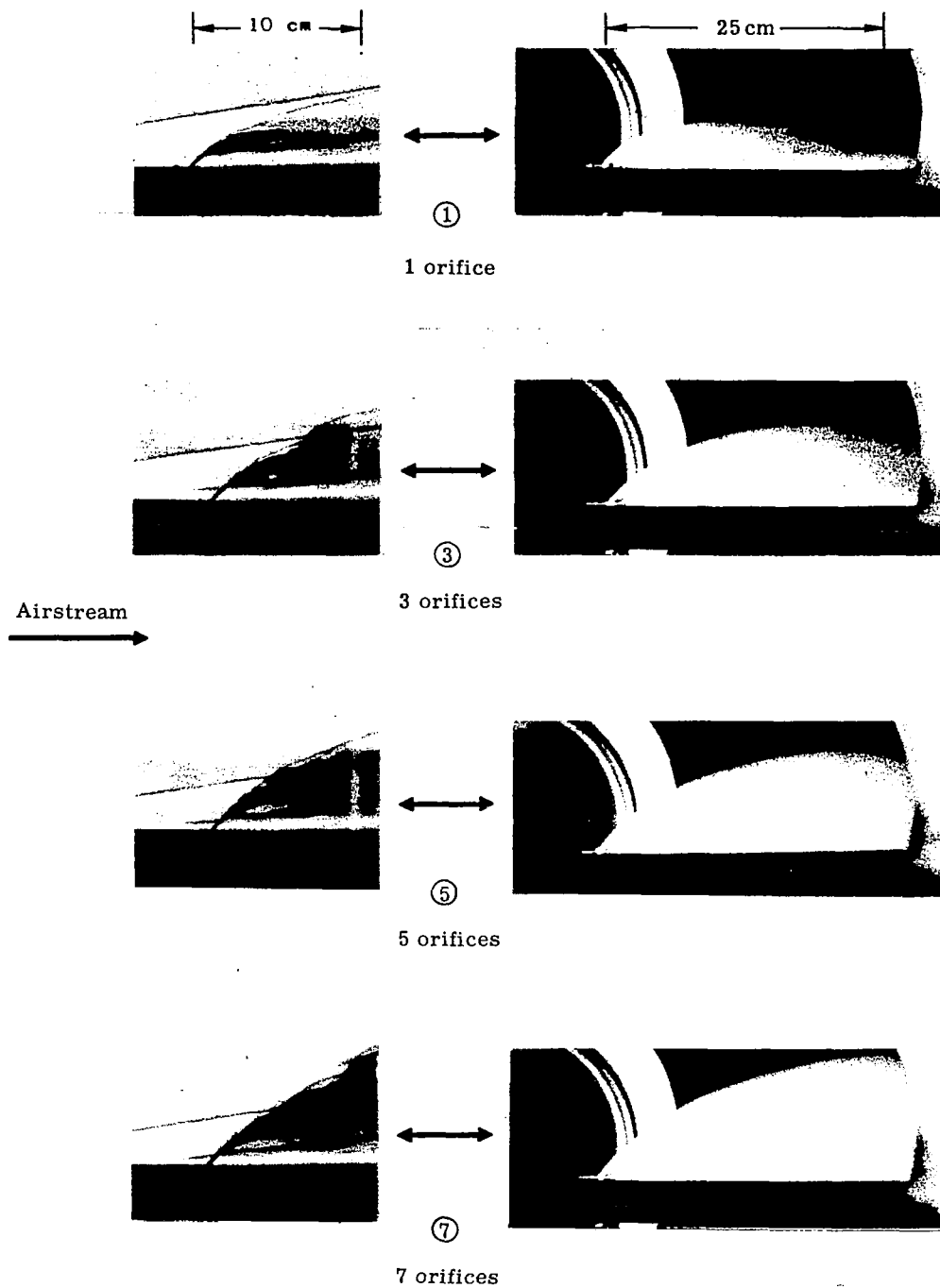
Figure 9.- Comparisons of measured and computed water-spray trajectories for single orifice on flat plate.



L-71-7157

(a) Side view; flat plate; effect of orifice diameter; $q_\infty = 47.4 \text{ kN/m}^2$; $|\bar{q}| = 39.7$.

Figure 10.- Photographs of water injection from single nozzles.



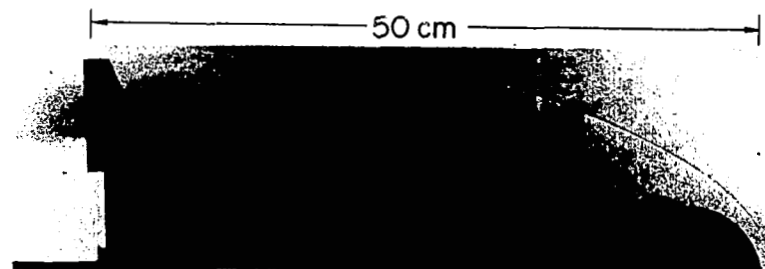
L-71-7158

(b) Side view; flat plate; effect of number of orifices;
 $D_j = 0.0508$ cm; $q_\infty = 31.6$ kN/m²; $\bar{q} = 60.5$.

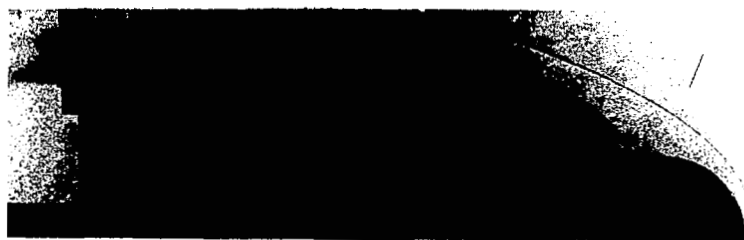
Figure 10.- Continued.



①
1 orifice



③
3 orifices
Airstream
←



⑤
5 orifices

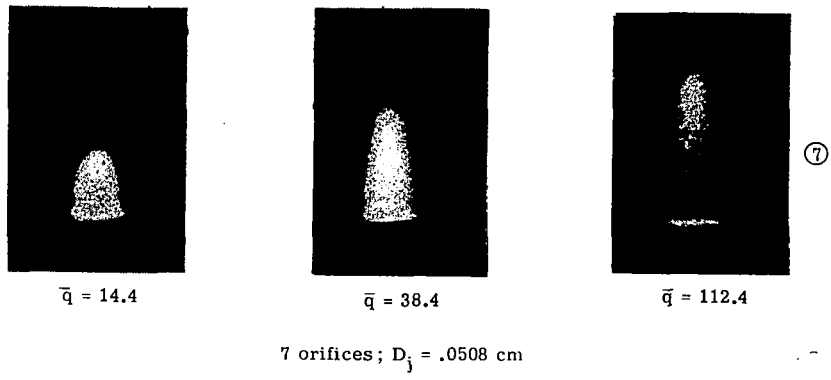
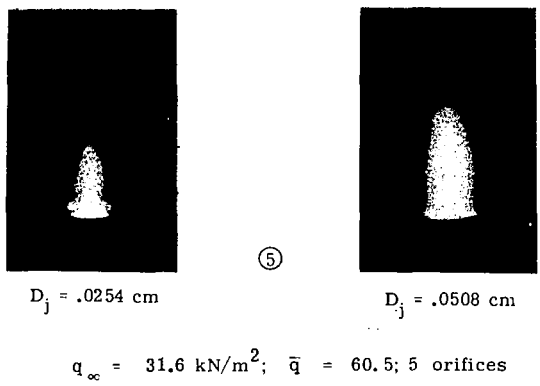
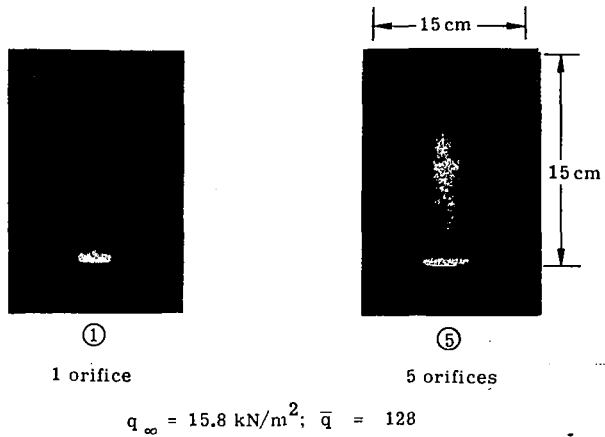


⑦
7 orifices

L-71-7159

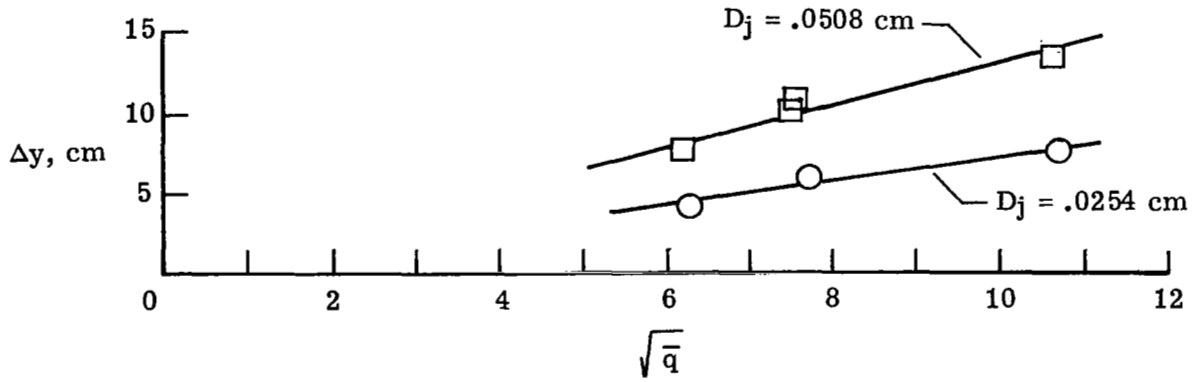
(c) Side view; hemisphere-cone; effect of number of orifices; $D_j = 0.0508$ cm; $q_\infty = 22.8$ kN/m²; $\bar{q} = 30.5$.

Figure 10.- Continued.

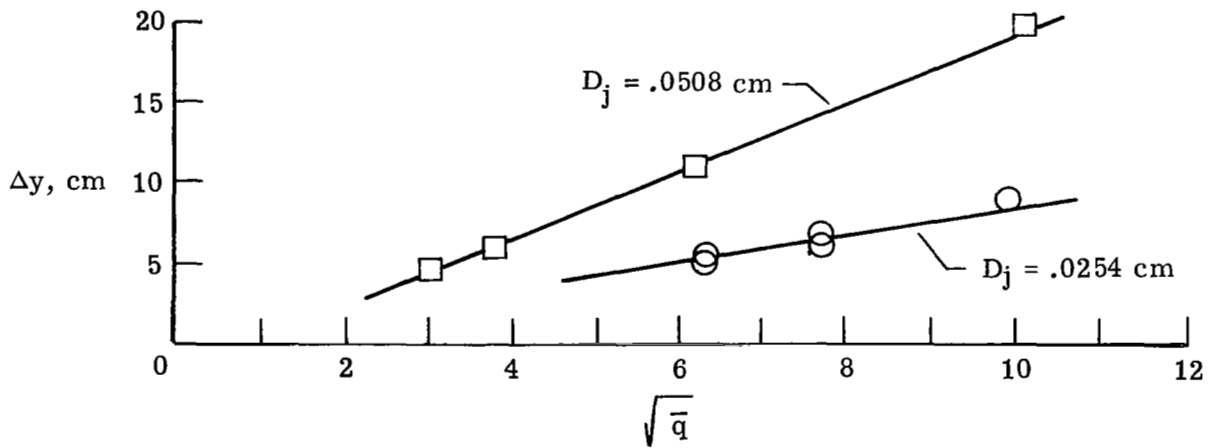


L-71-7160

(d) Spray cross section; flat plate.
Figure 10.- Concluded.

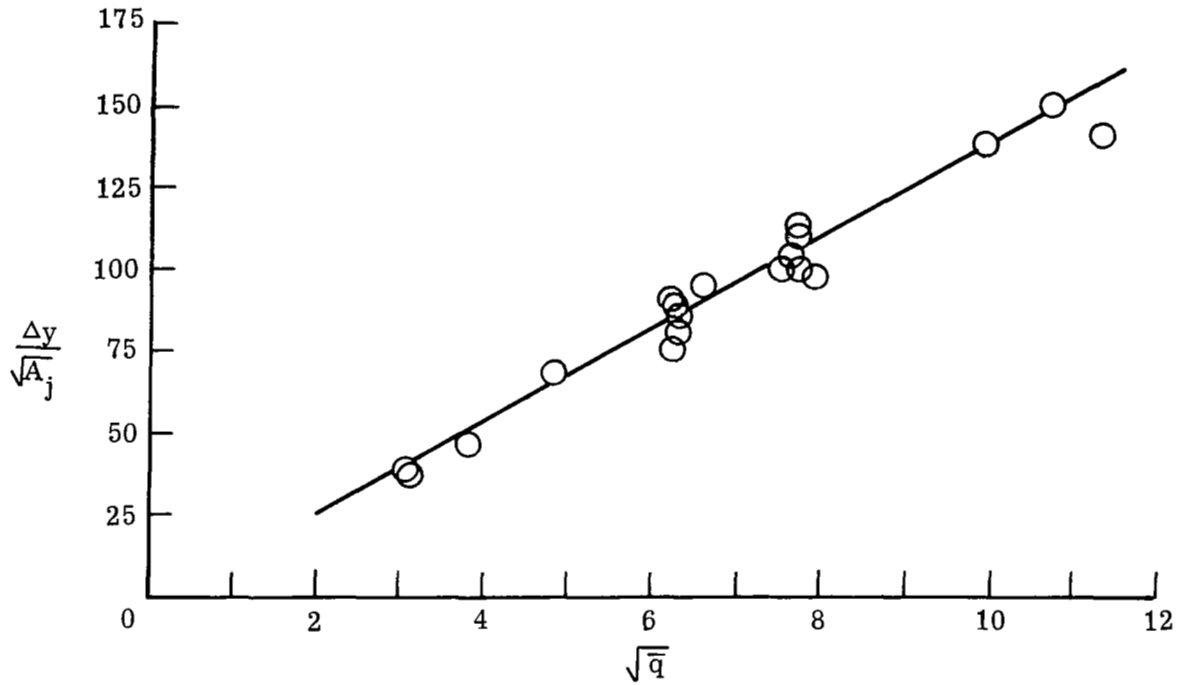


(a) Five orifices.

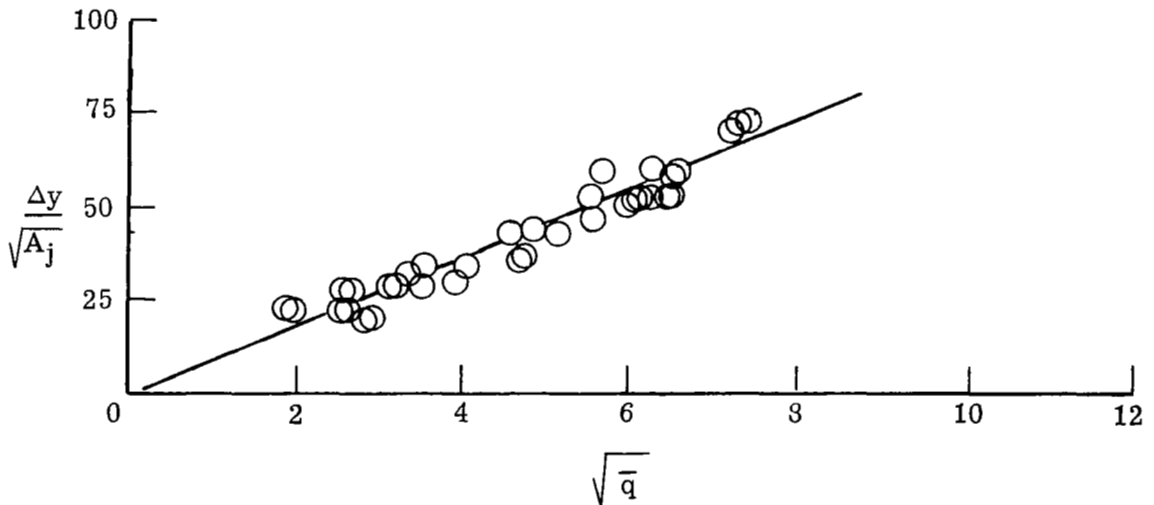


(b) Seven orifices.

Figure 11.- Effect of orifice diameter on penetration for water injection through single nozzles of five or seven orifices from flat plate.



(a) Flat plate; five or seven orifices for $D_j = 0.0254$ cm; one, three, five, or seven orifices for $D_j = 0.0508$ cm.



(b) Hemisphere-cone; three, five, or seven orifices; $D_j = 0.0508$ cm.

Figure 12.- Correlation of nondimensional maximum water penetration with single nozzles.

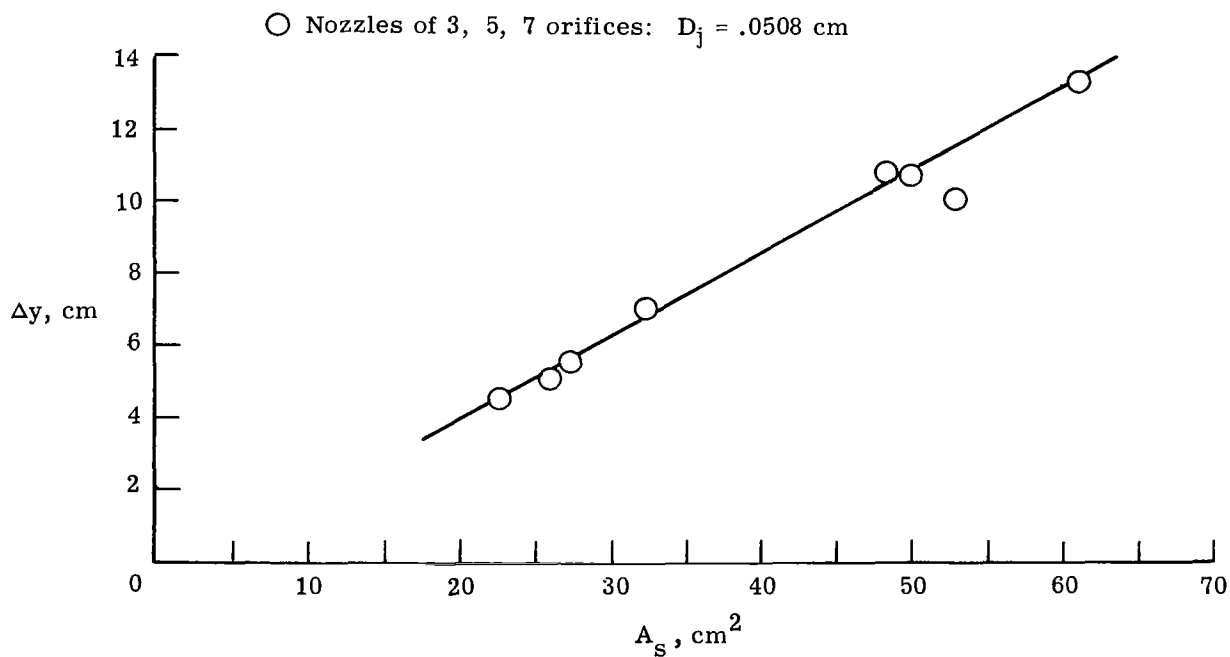
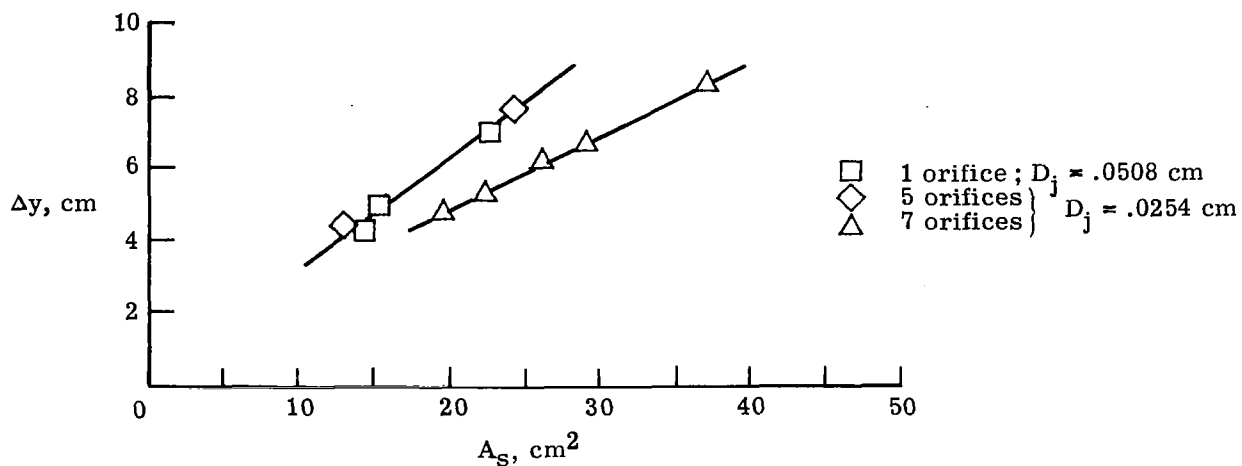
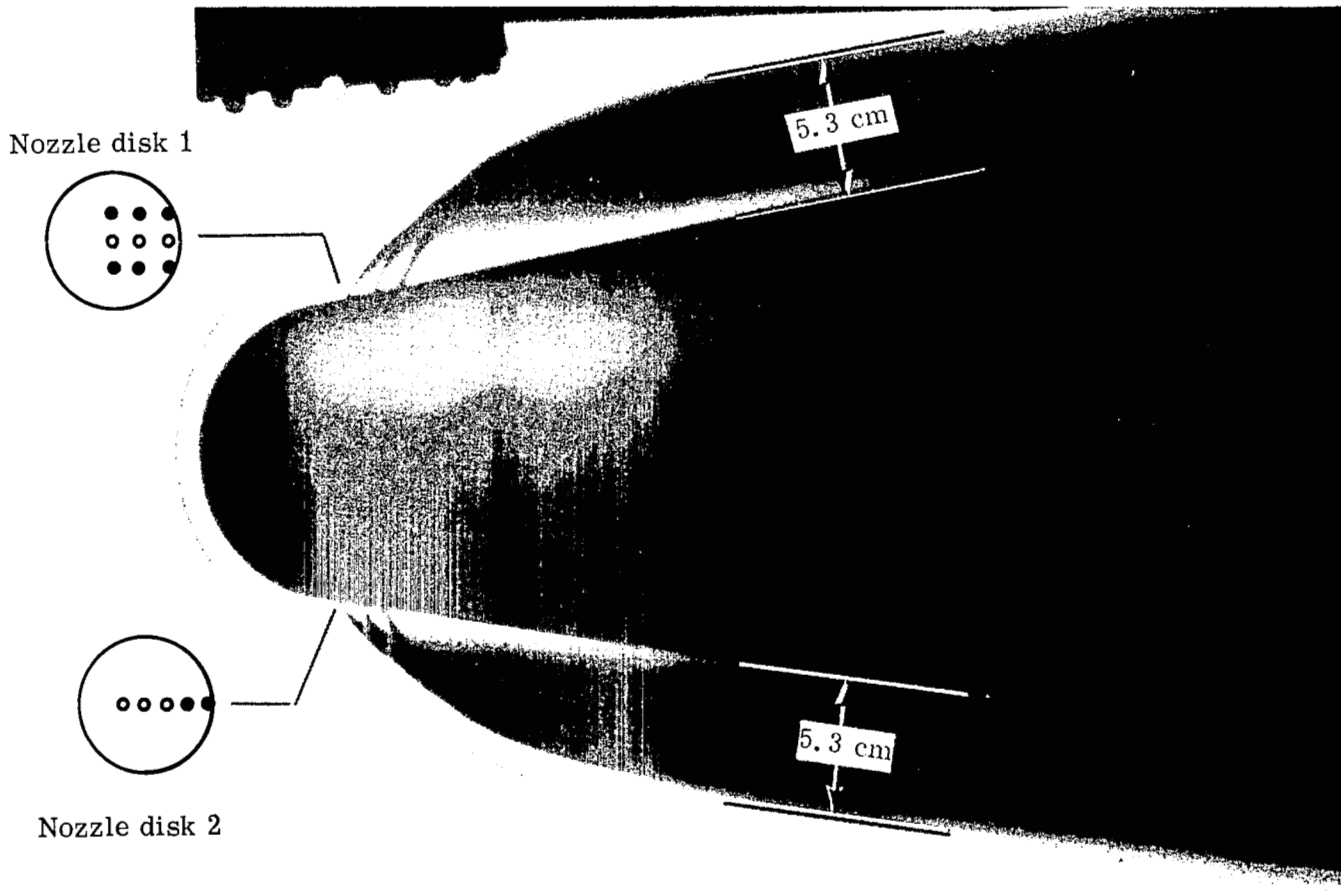


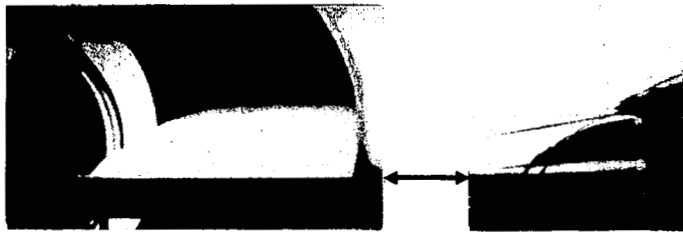
Figure 13.- Maximum water penetration versus spray cross-section area for single nozzles on flat plate.



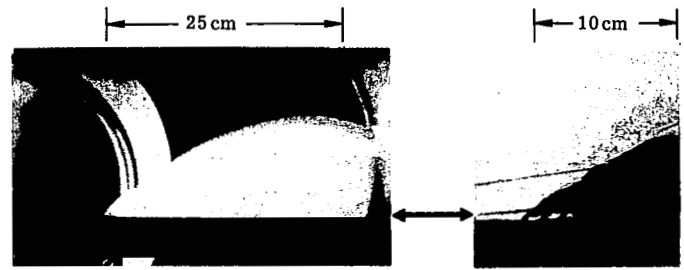
(a) Side view; water; effect of nozzle spacing.

L-71-7161

Figure 14.- Photographs of liquid injection with single rows of nozzles.

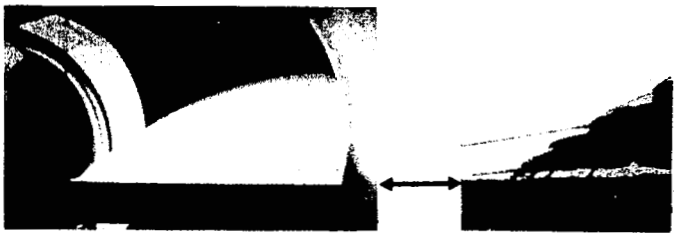


⑤ ⑤

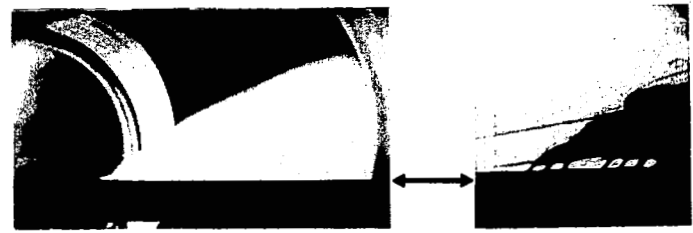


⑦ ⑦ ⑤

Airstream →



⑤ ⑤ ⑤ ⑤



⑦ ⑦ ⑤ ⑤ ③ ③

$$q_{\infty} = 47.4 \text{ kN/m}^2; \bar{q} = 20.3; D_j = .0508 \text{ cm}$$

(b) Side view; water injection from flat plate.

L-71-7162

Figure 14.- Continued.



$q_{\infty} = 16.3 \text{ kN/m}^2; \bar{q} = 5.2; D_j = .0254 \text{ cm}$

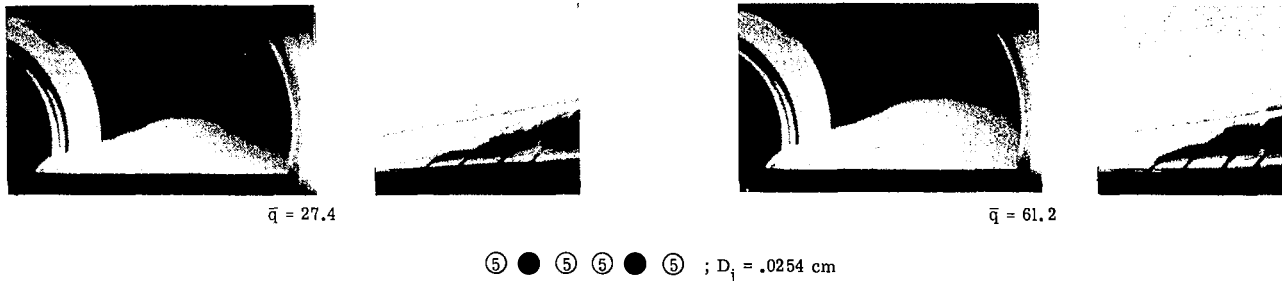
Nozzle pattern effect

Airstream →



$q_{\infty} = 47.4 \text{ kN/m}^2; \bar{q} = 4.5$

Effect of nozzle pattern and orifice diameter



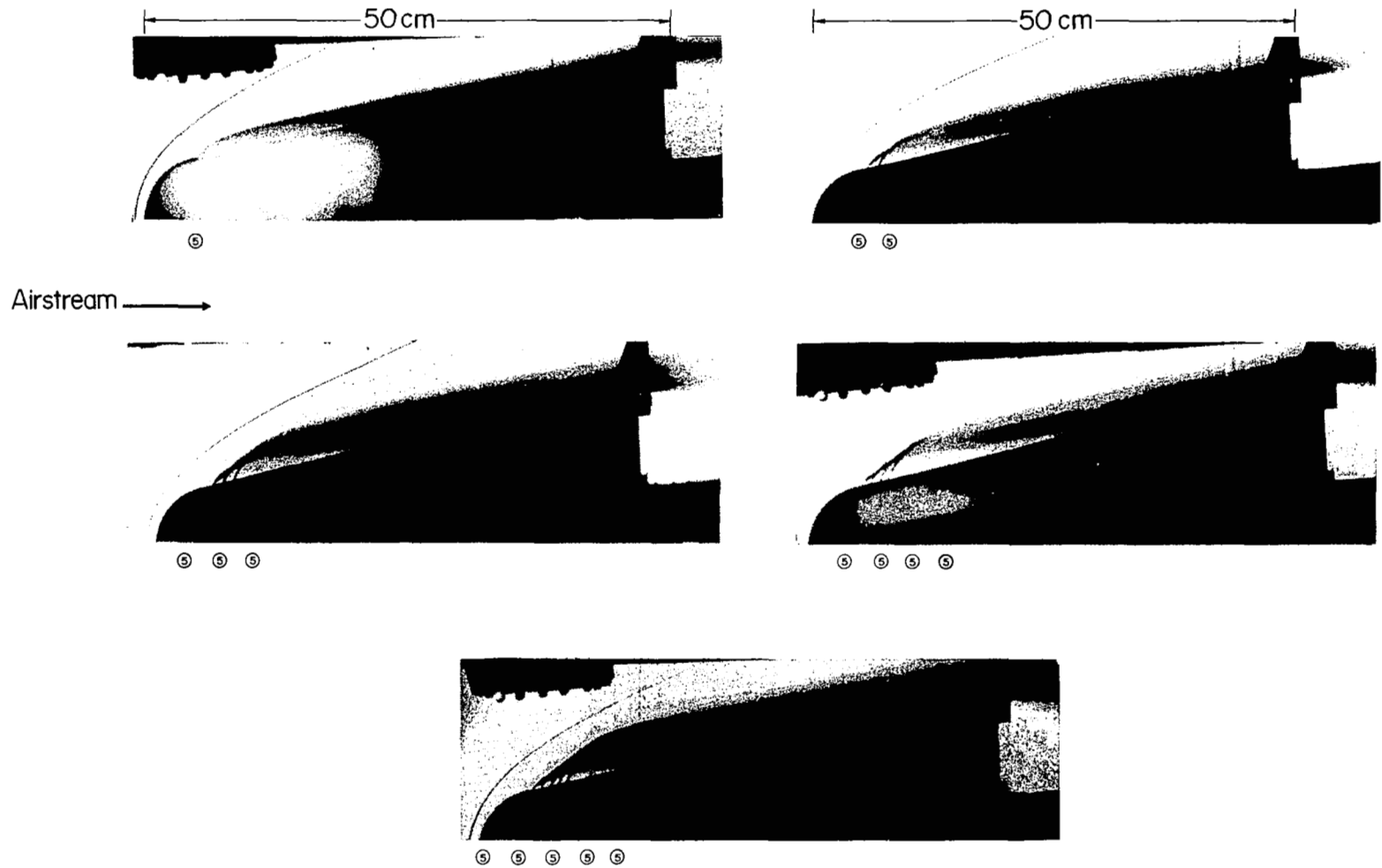
$\bar{q} = 27.4$; $D_j = .0254 \text{ cm}$; $\bar{q} = 61.2$

Dynamic-pressure ratio effect

L-71-7163

(c) Side view; Freon E-3 injection from flat plate.

Figure 14.- Continued.

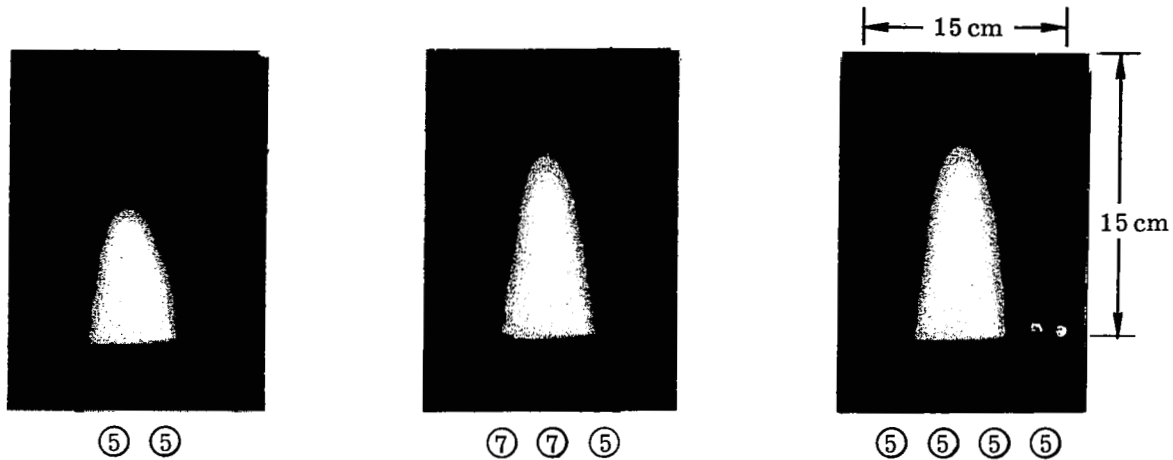


5 orifices per nozzle; $D_j = .0508 \text{ cm}$; $q_w = 43.4 \text{ kN/m}^2$; $\bar{q} = 7.0$

(d) Side view; water injection from hemisphere-cone.

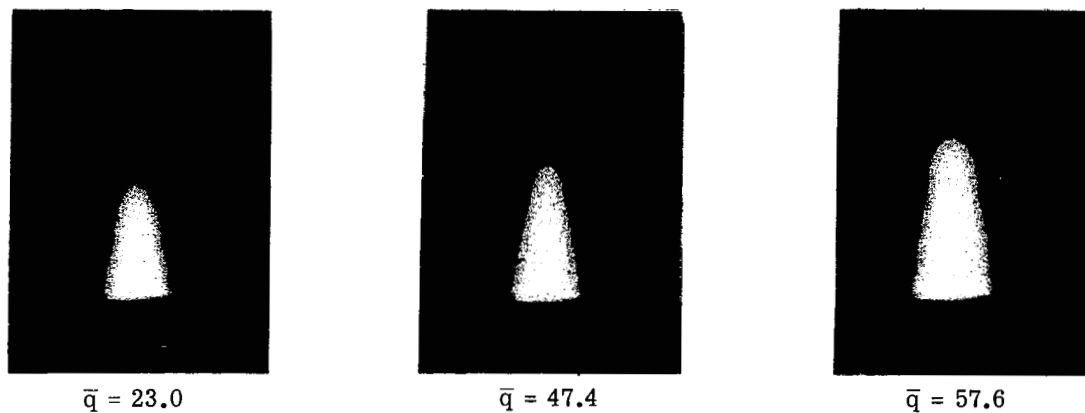
L-71-7164

Figure 14.- Continued.



$$q_{\infty} = 47.4 \text{ kN/m}^2; \bar{q} = 20.3; D_j = .0508 \text{ cm}$$

Nozzle pattern effect



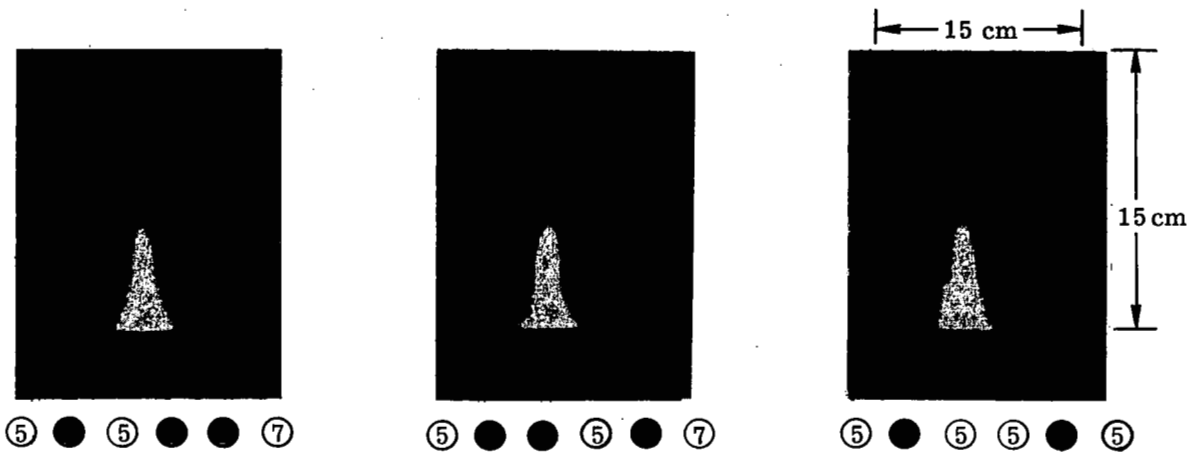
$$\textcircled{1} \textcircled{1} \textcircled{1} ; D_j = .0508 \text{ cm}$$

Dynamic-pressure ratio effect

(e) Water-spray cross section; flat plate.

L-71-7165

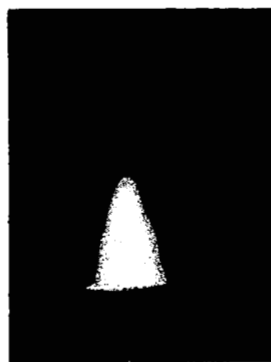
Figure 14.- Continued.



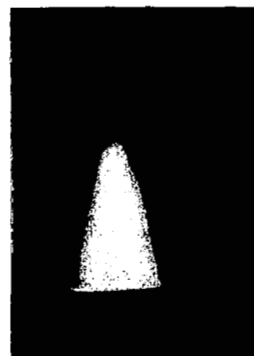
$$q_{\infty} = 16.3 \text{ kN/m}^2$$

$$\bar{q}_{\infty} = 16.3 \text{ kN/m}^2; \bar{q} = 27.4; D_j = .0254 \text{ cm}$$

Nozzle pattern effect



$\bar{q} = 20.3$



$\bar{q} = 61.3$

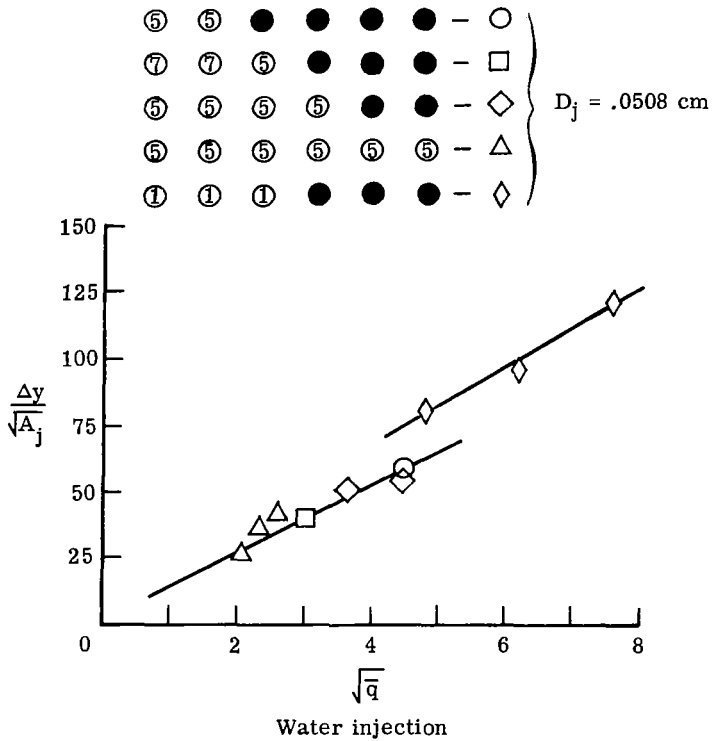
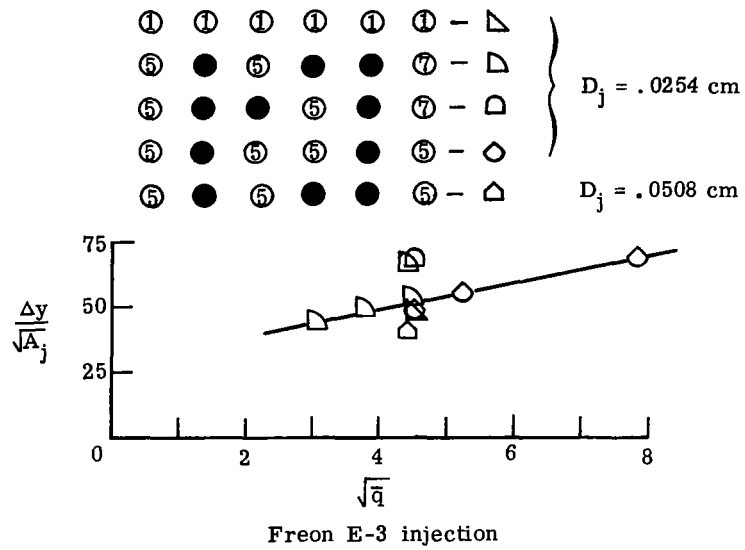
$$(5) \bullet (5) (5) \bullet (5) ; D_j = .0254 \text{ cm}$$

Dynamic-pressure ratio effect

(f) Freon E-3 spray cross section; flat plate.

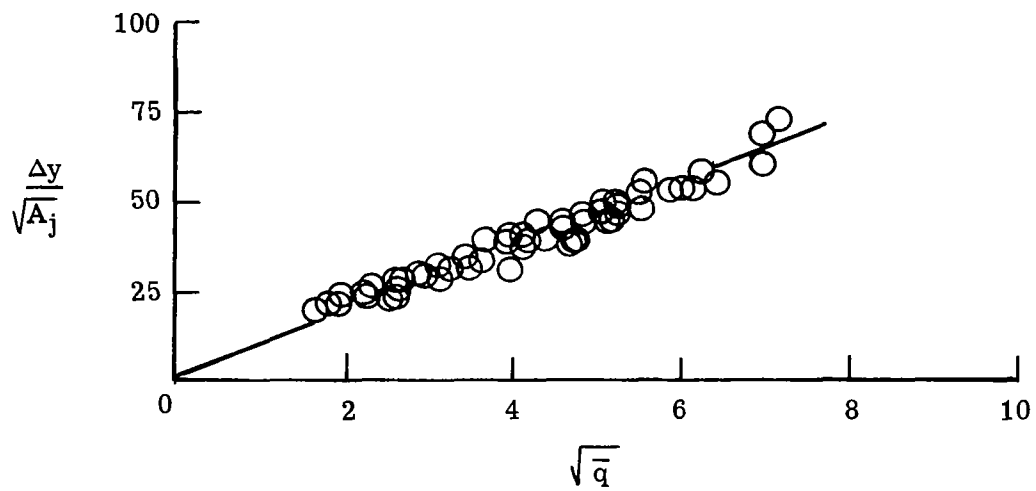
L-71-7166

Figure 14.- Concluded.



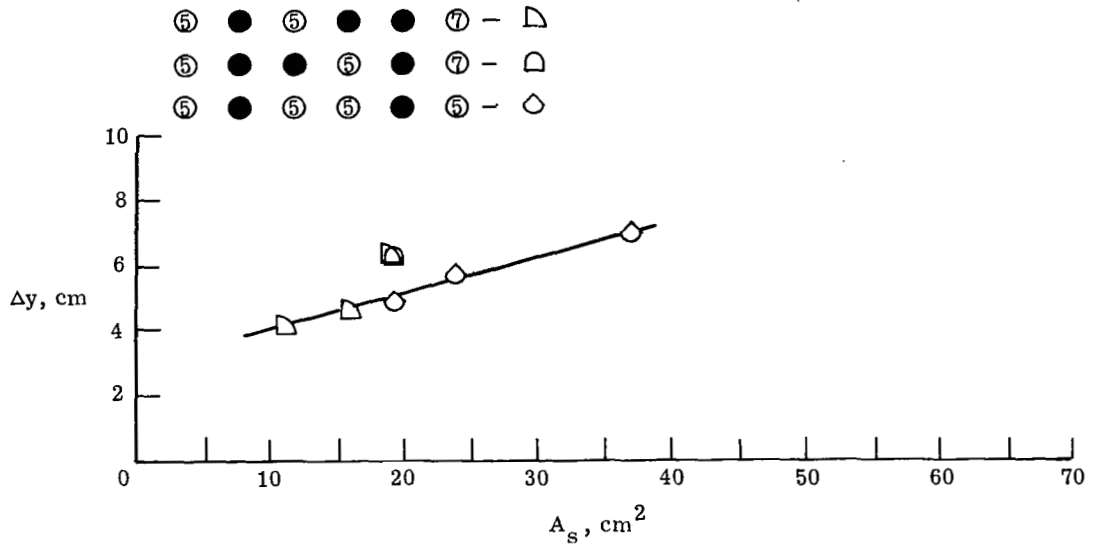
(a) Flat plate; water and Freon E-3 injection.

Figure 15.- Correlation of nondimensional maximum liquid penetration with single rows of in-line nozzles.

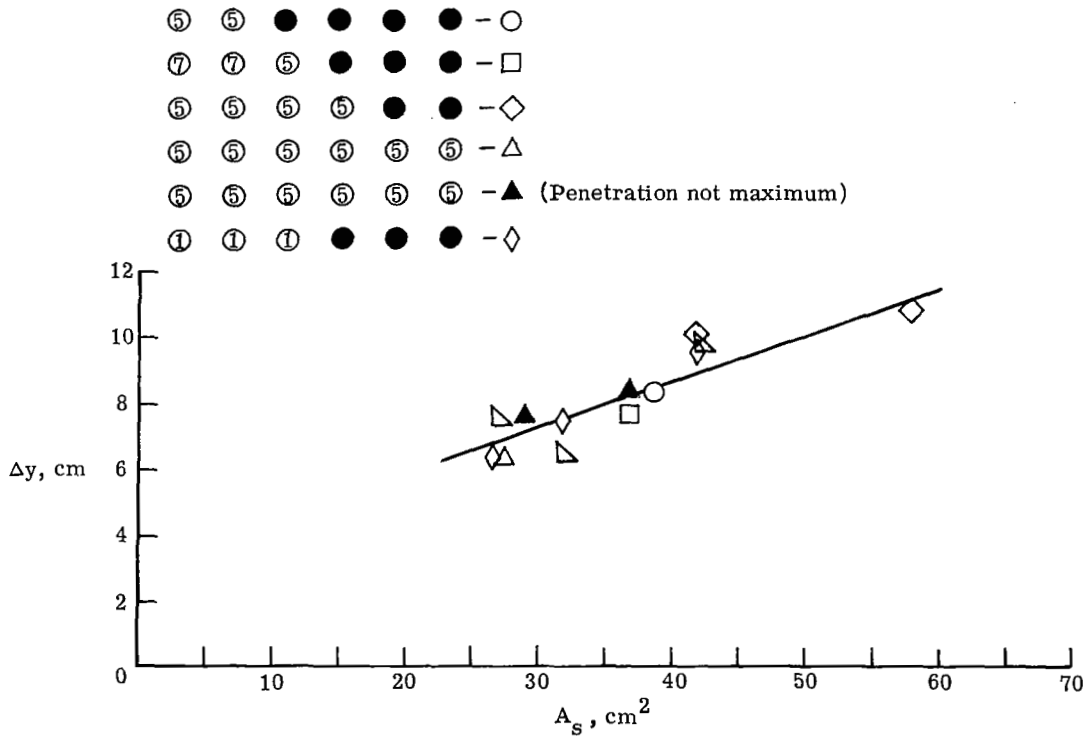


(b) Hemisphere-cone; water injection. One, two, three, four, or five nozzles; five orifices per nozzle; $D_j = 0.0508$ cm.

Figure 15.- Concluded.

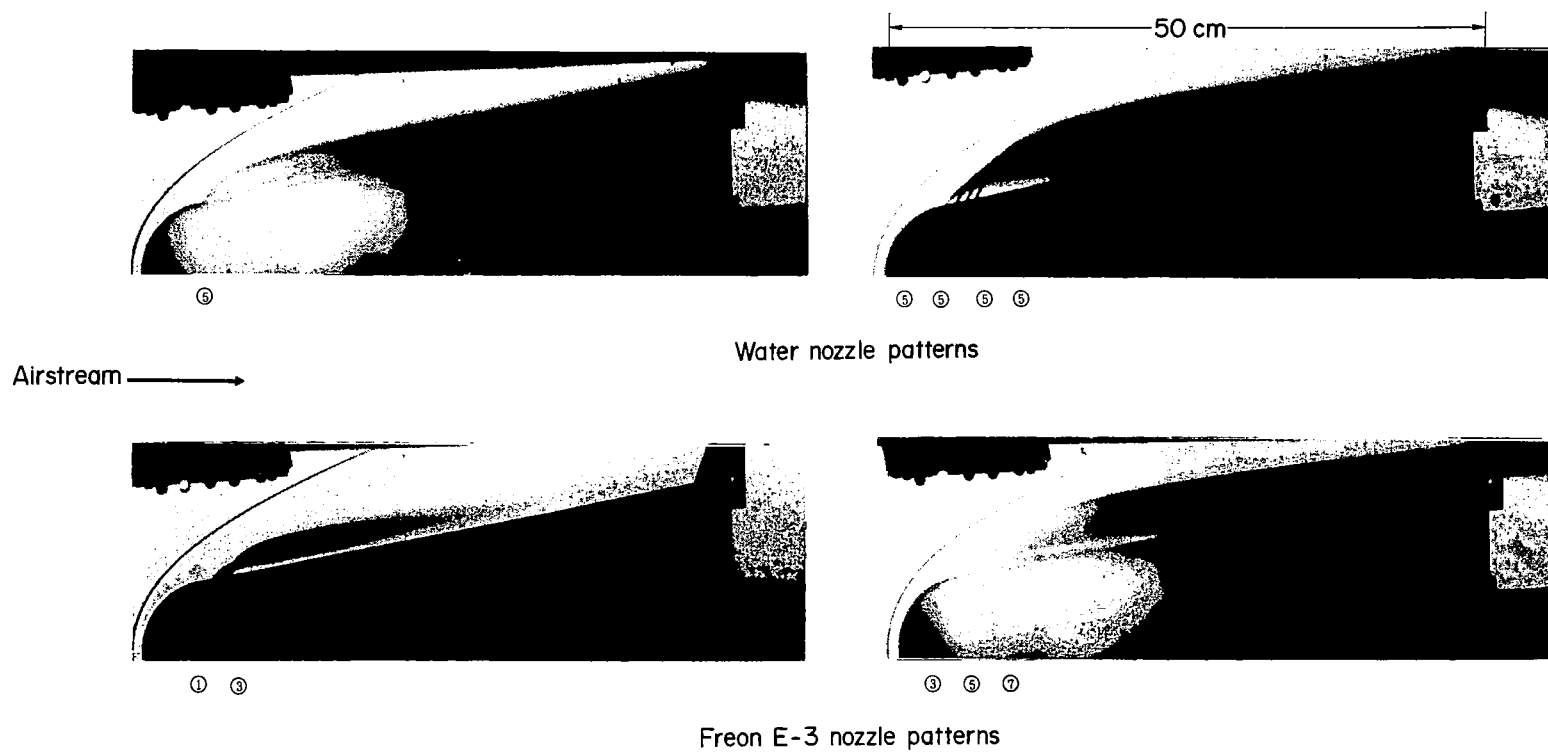


(a) Freon E-3 injection; $D_j = 0.0254 \text{ cm}$.



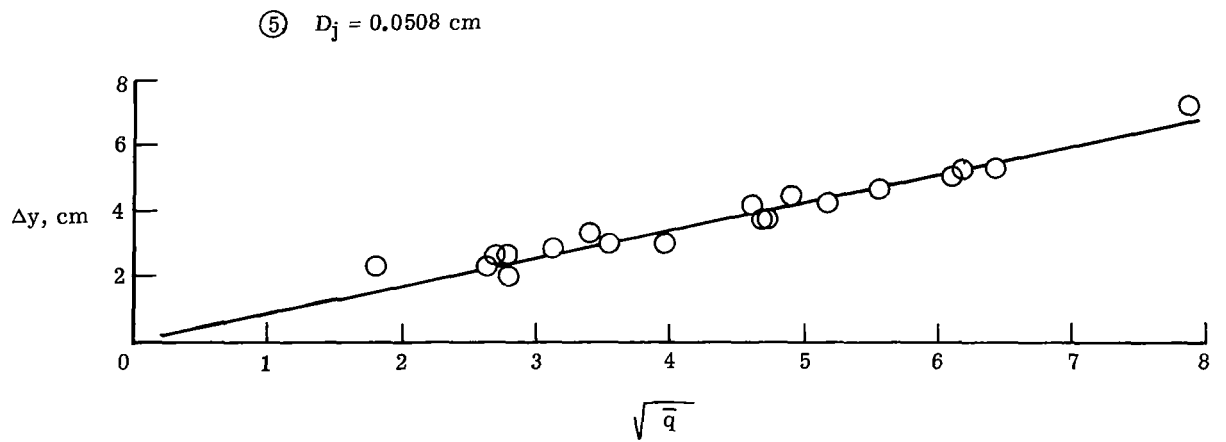
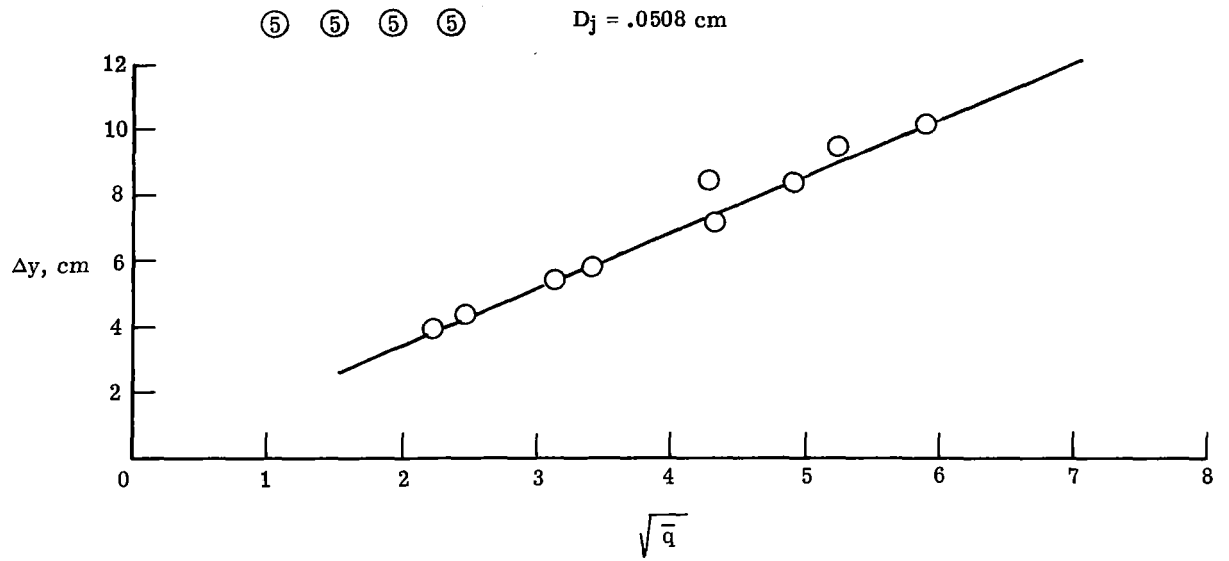
(b) Water injection; $D_j = 0.0508 \text{ cm}$.

Figure 16.- Maximum liquid penetration versus spray cross-section area for in-line nozzles on flat plate.



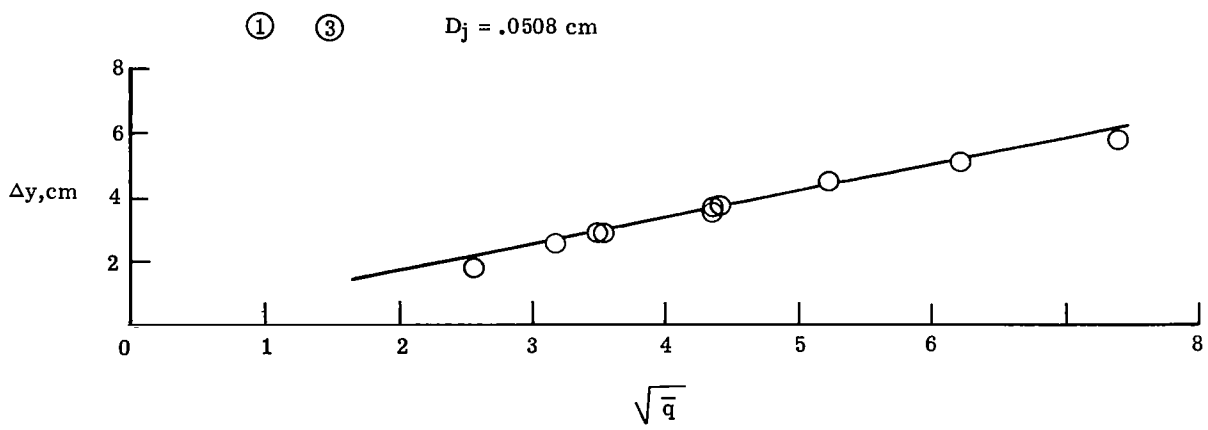
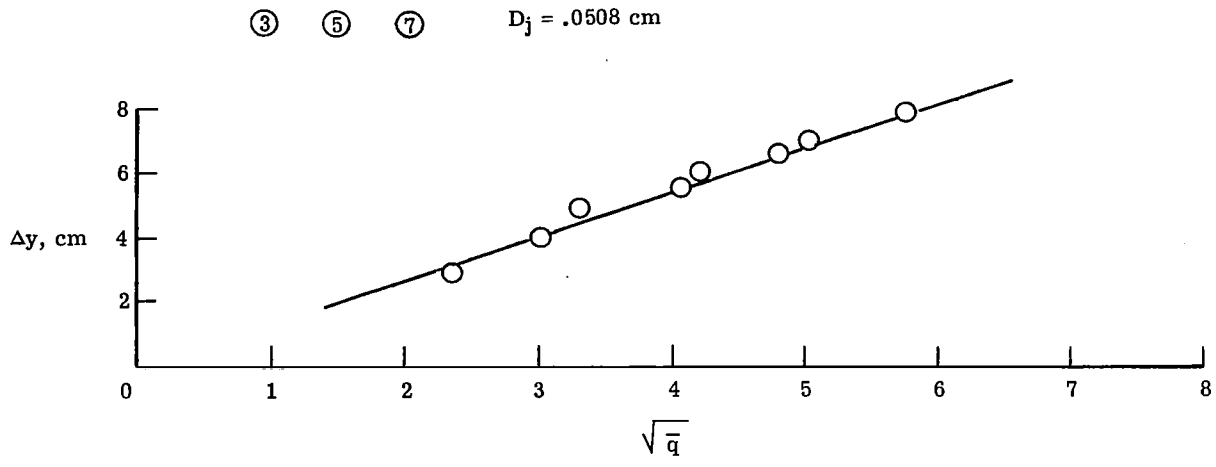
L-71-7167

Figure 17.- Photographs of tests with RAM C-III nozzles; $q_{\infty} = 64.8 \text{ kN/m}^2$; $p_j = 1.34 \text{ MN/m}^2$; $D_j \approx 0.0508 \text{ cm}$.



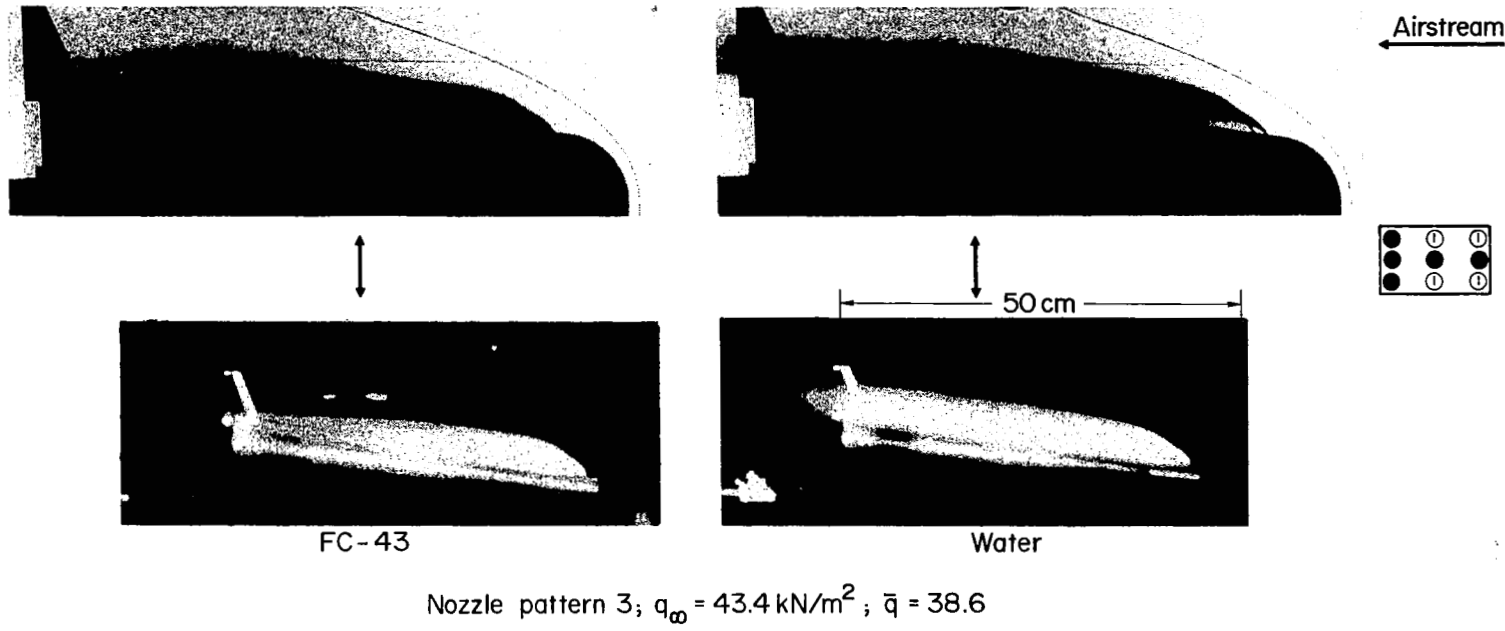
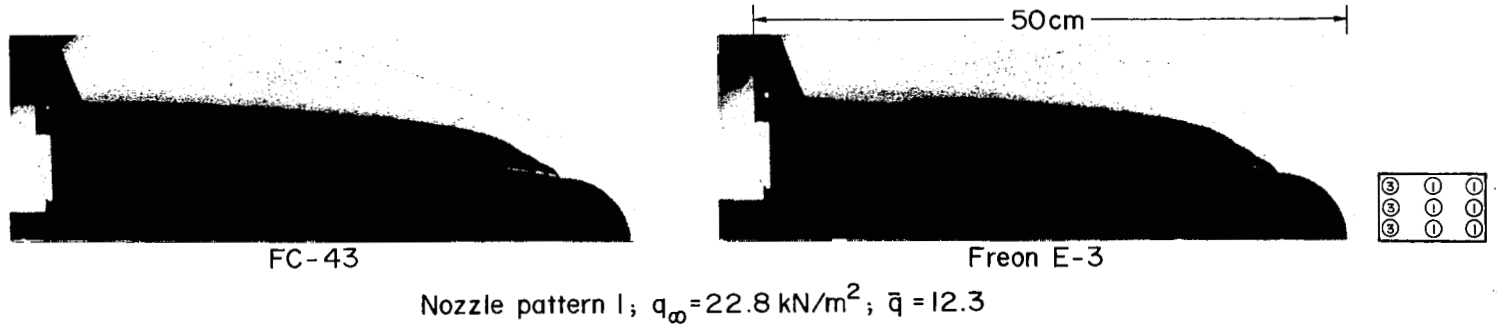
(a) Water-injection nozzle patterns.

Figure 18.- Maximum penetration for RAM C-III nozzles.



(b) Freon E-3 injection nozzle patterns.

Figure 18.- Concluded.

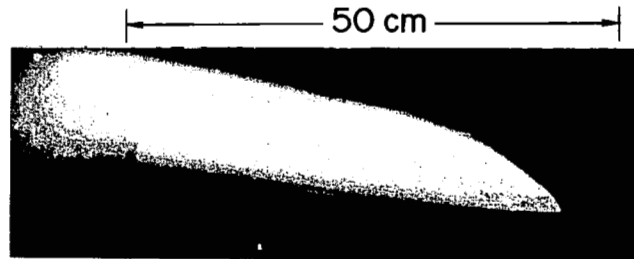


(a) Comparisons with different liquids; $D_j = 0.0508 \text{ cm}$.
Figure 19.- Photographs of injection with nozzle patterns 1 to 4.

L-71-7168

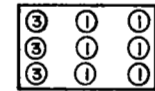


FC-75; $D_j = .0254$ cm



Freon E-3; $D_j = .0508$ cm

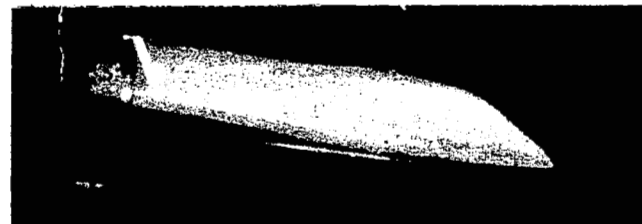
Nozzle pattern 1; $q_{\infty} = 22.8$ kN/m²; $\bar{q} = 38.8$



Airstream ←

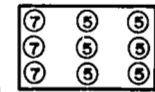


$D_j = .0254$ cm



$D_j = .0508$ cm

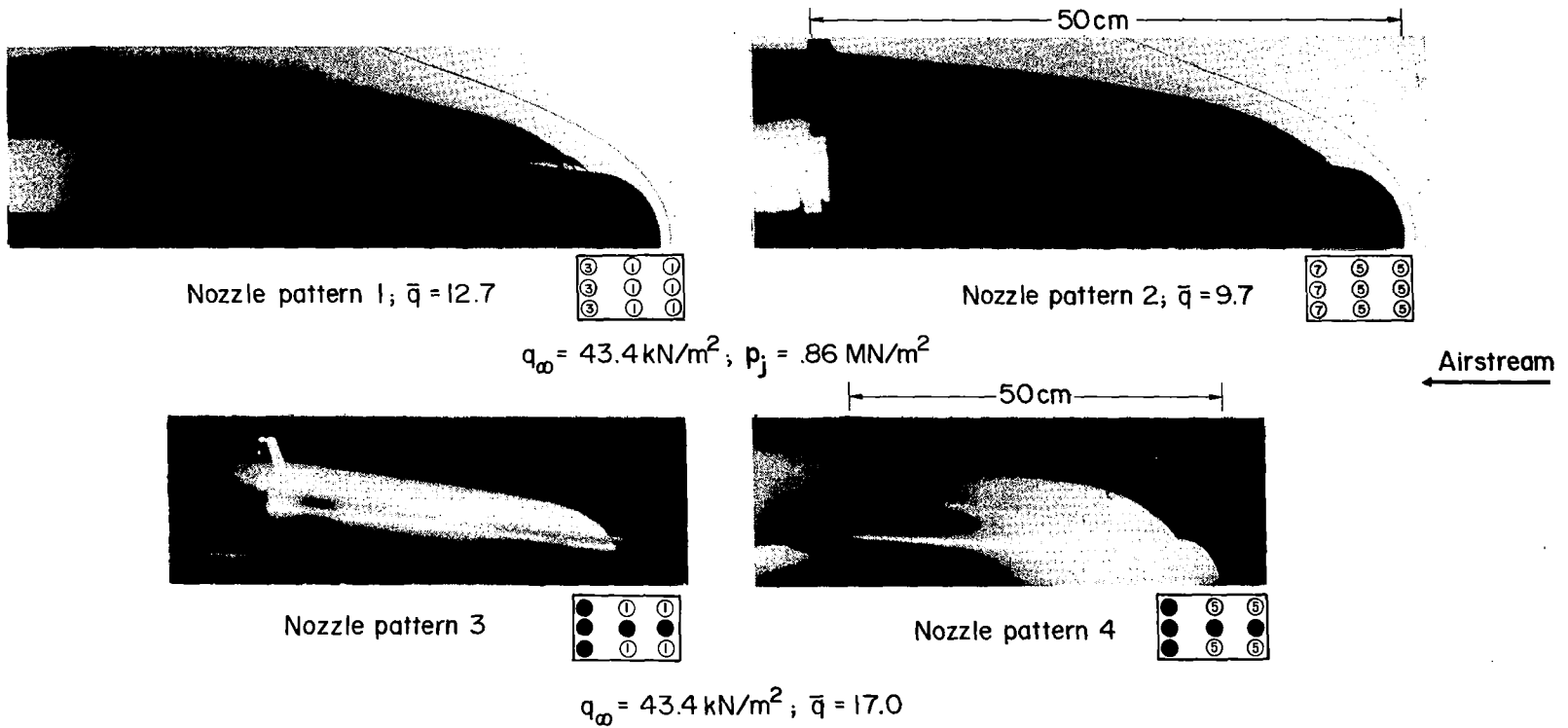
Nozzle pattern 2; $q_{\infty} = 22.8$ kN/m²; $\bar{q} = 20.5$; Water



L-71-7169

(b) Comparisons with two different orifice diameters.

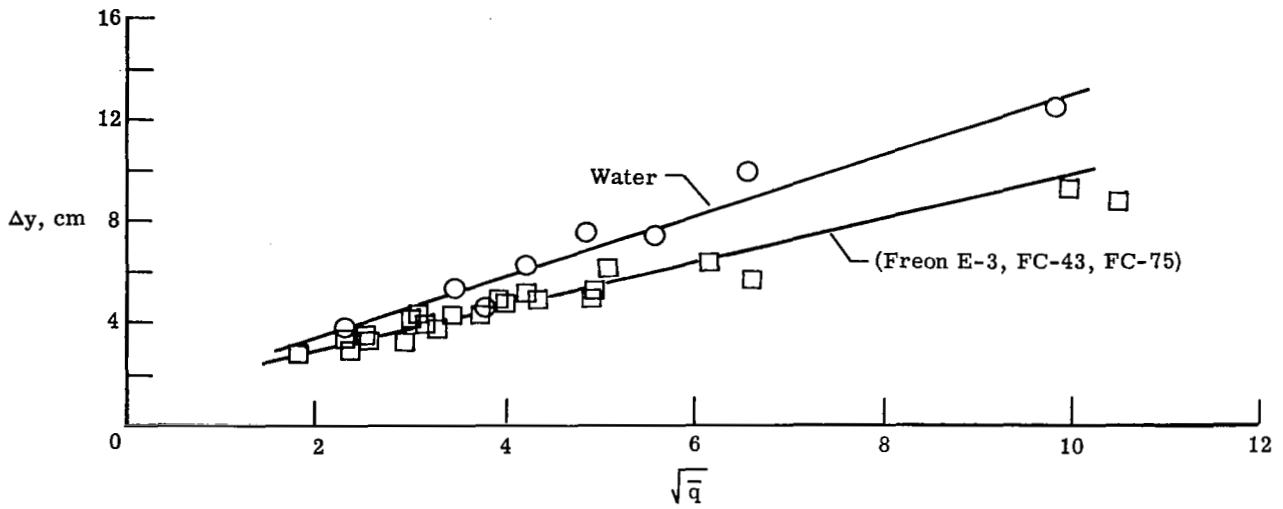
Figure 19.- Continued.



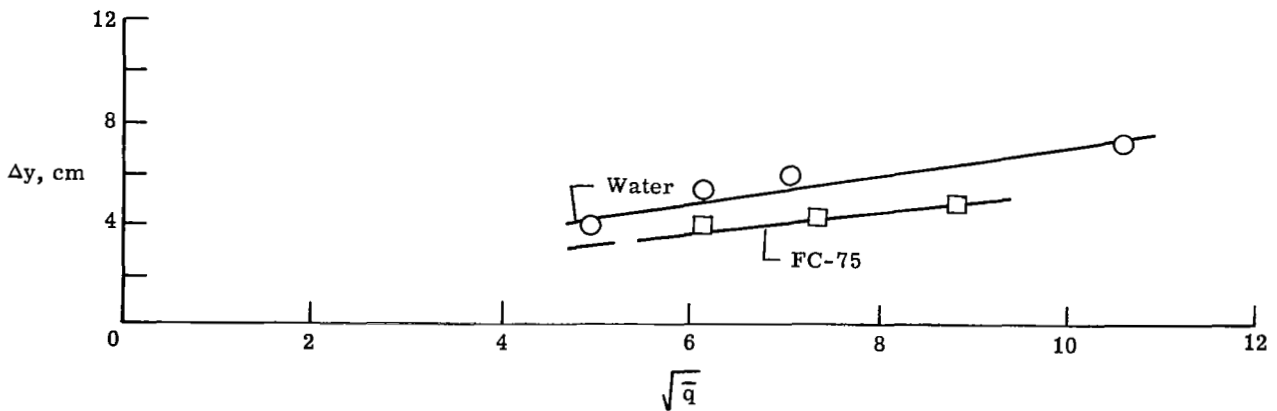
L-71-7170

(c) Comparisons with different numbers of orifices per nozzle; water.

Figure 19.- Concluded.

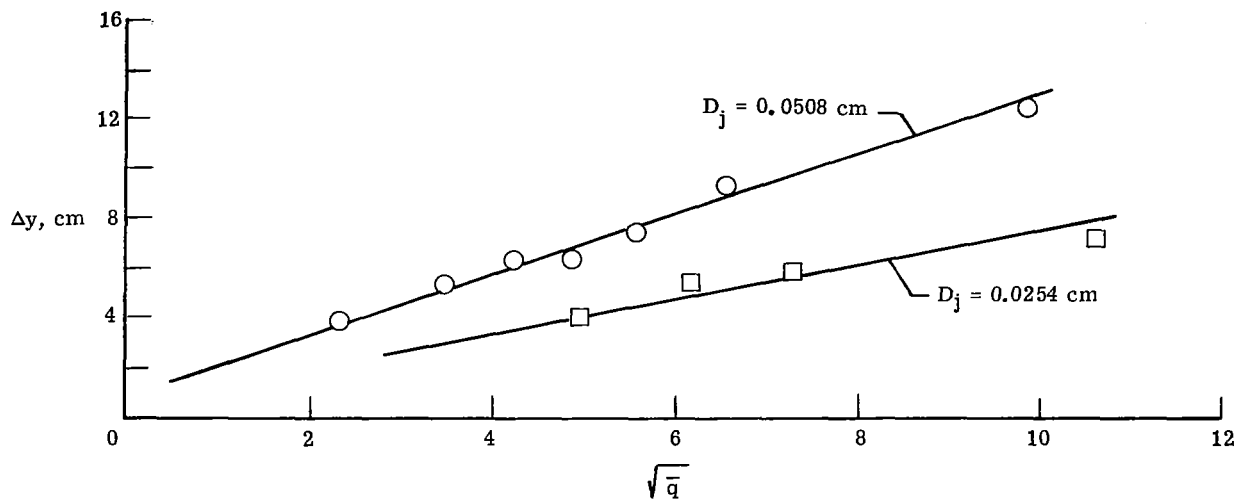


(a) Effect of liquid; nozzle pattern 1; $D_j = 0.0508$ cm.

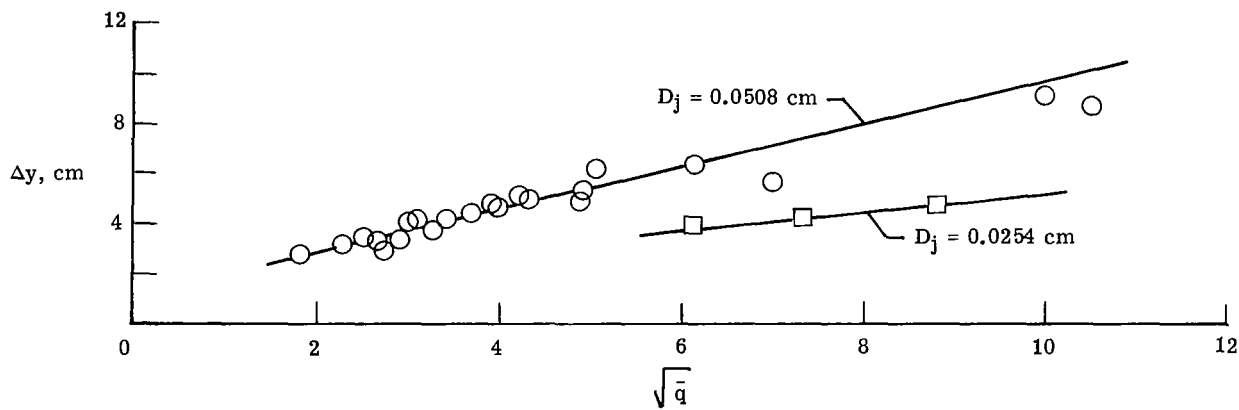


(b) Effect of liquid; nozzle pattern 1; $D_j = 0.0254$ cm.

Figure 20.- Comparison plots of maximum penetration for nozzle patterns 1 and 2.

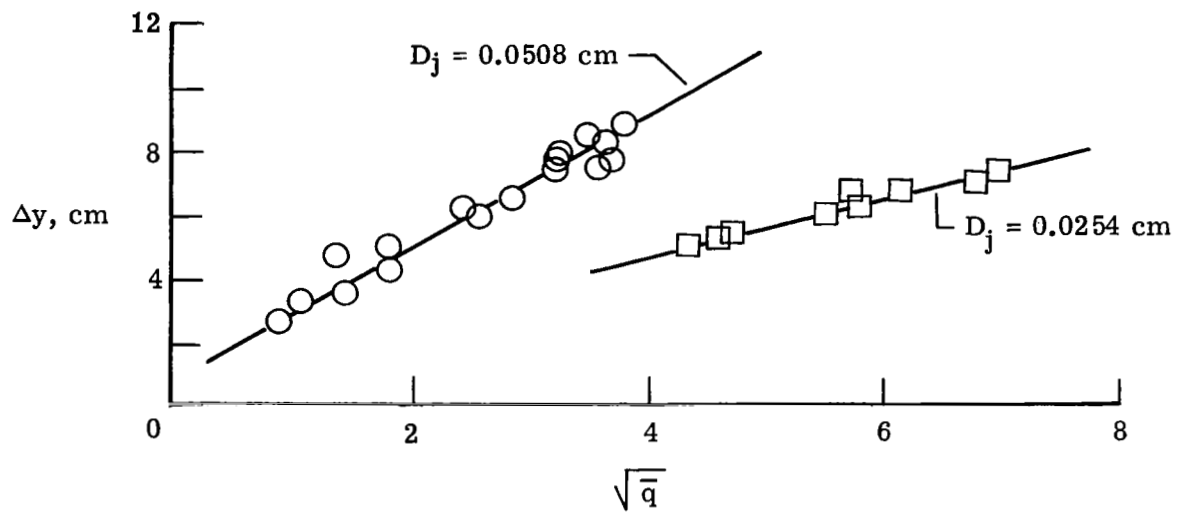


(c) Effect of orifice diameter; nozzle pattern 1; water.



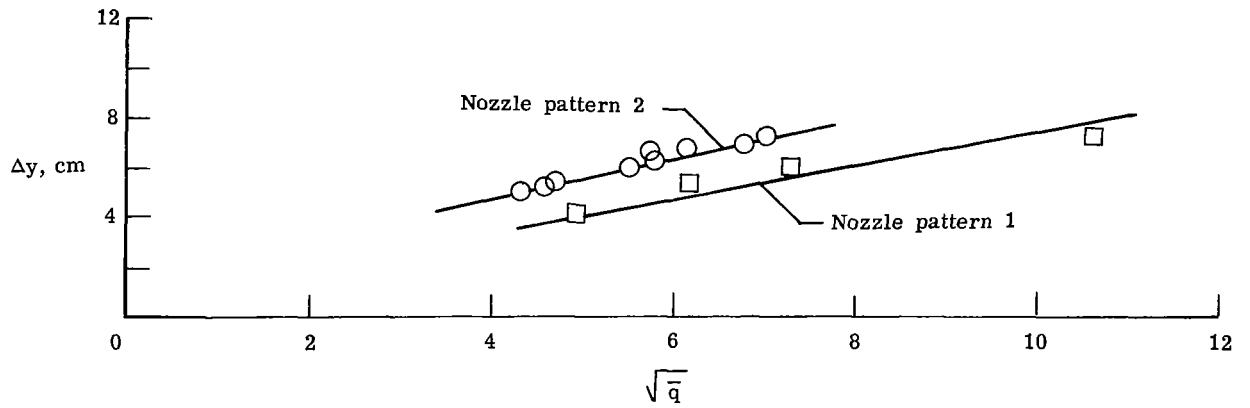
(d) Effect of orifice diameter; nozzle pattern 1; Freon E-3, FC-43, FC-75.

Figure 20.- Continued.

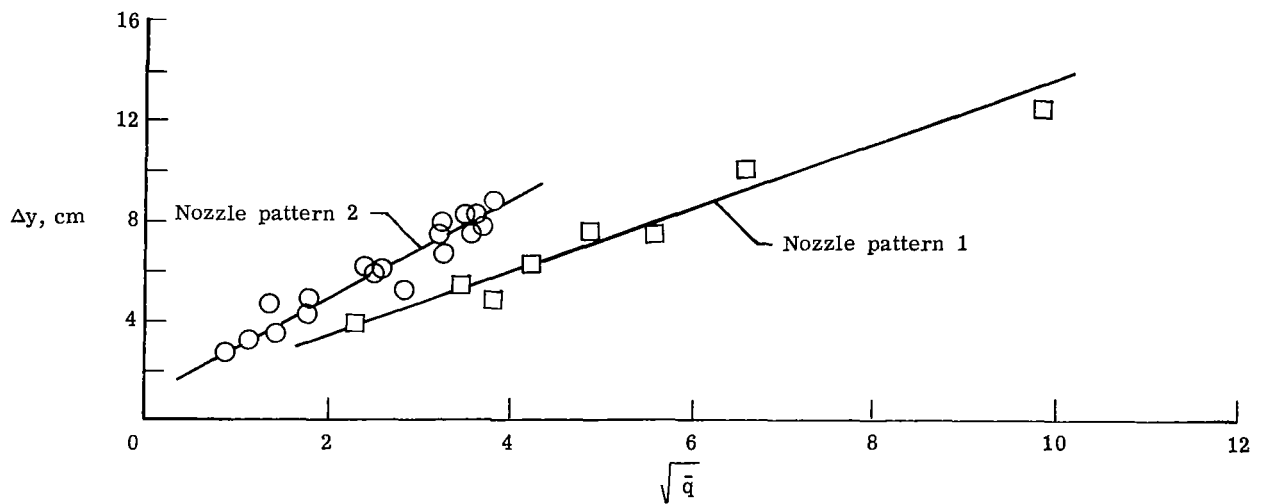


(e) Effect of orifice diameter; nozzle pattern 2; water.

Figure 20.- Continued.

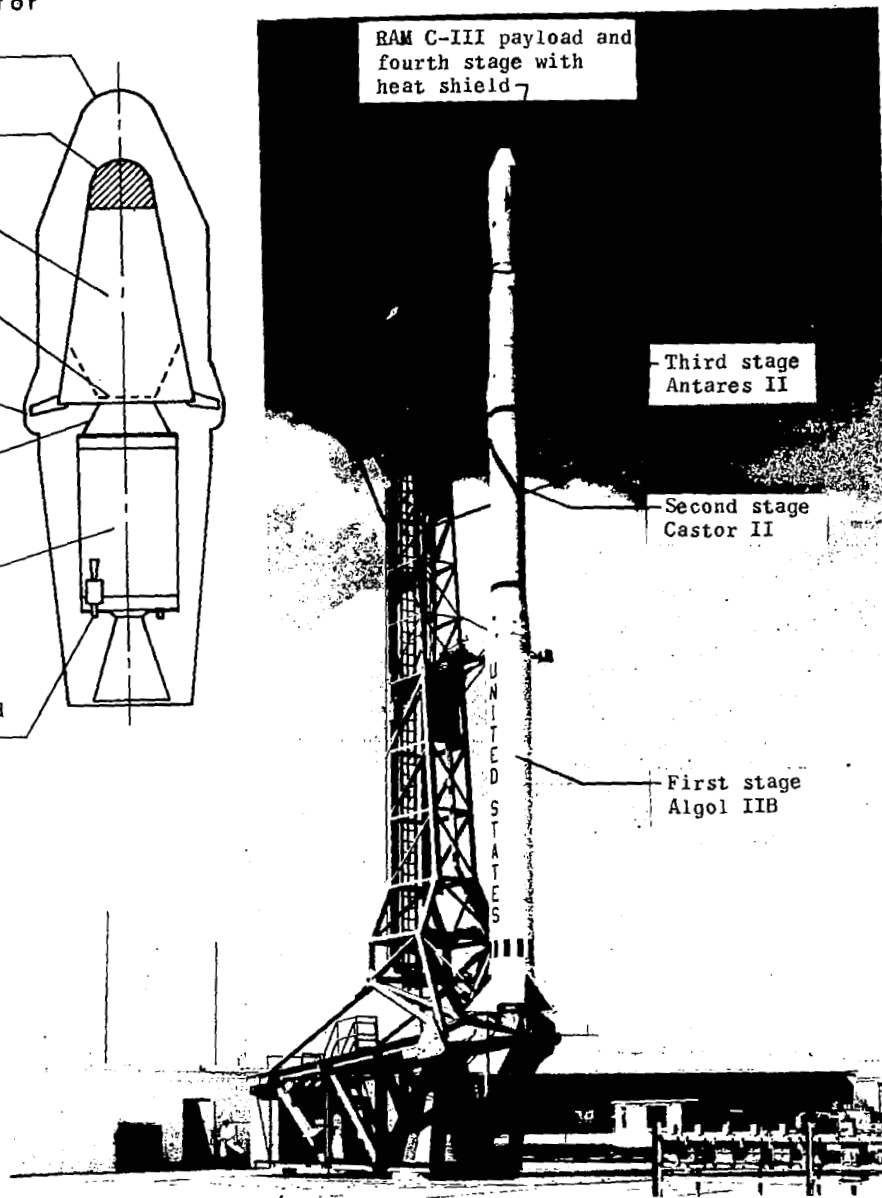
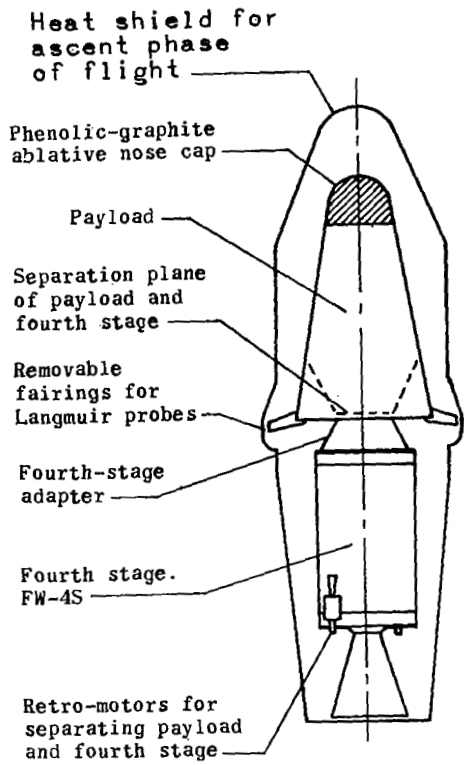


(f) Effect of number of orifices per nozzle; water; $D_j = 0.0508$ cm.



(g) Effect of number of orifices per nozzle; water; $D_j = 0.0254$ cm.

Figure 20.- Concluded.



L-71-7171

Figure 21.- Boost vehicle and spacecraft for RAM C-III flight.

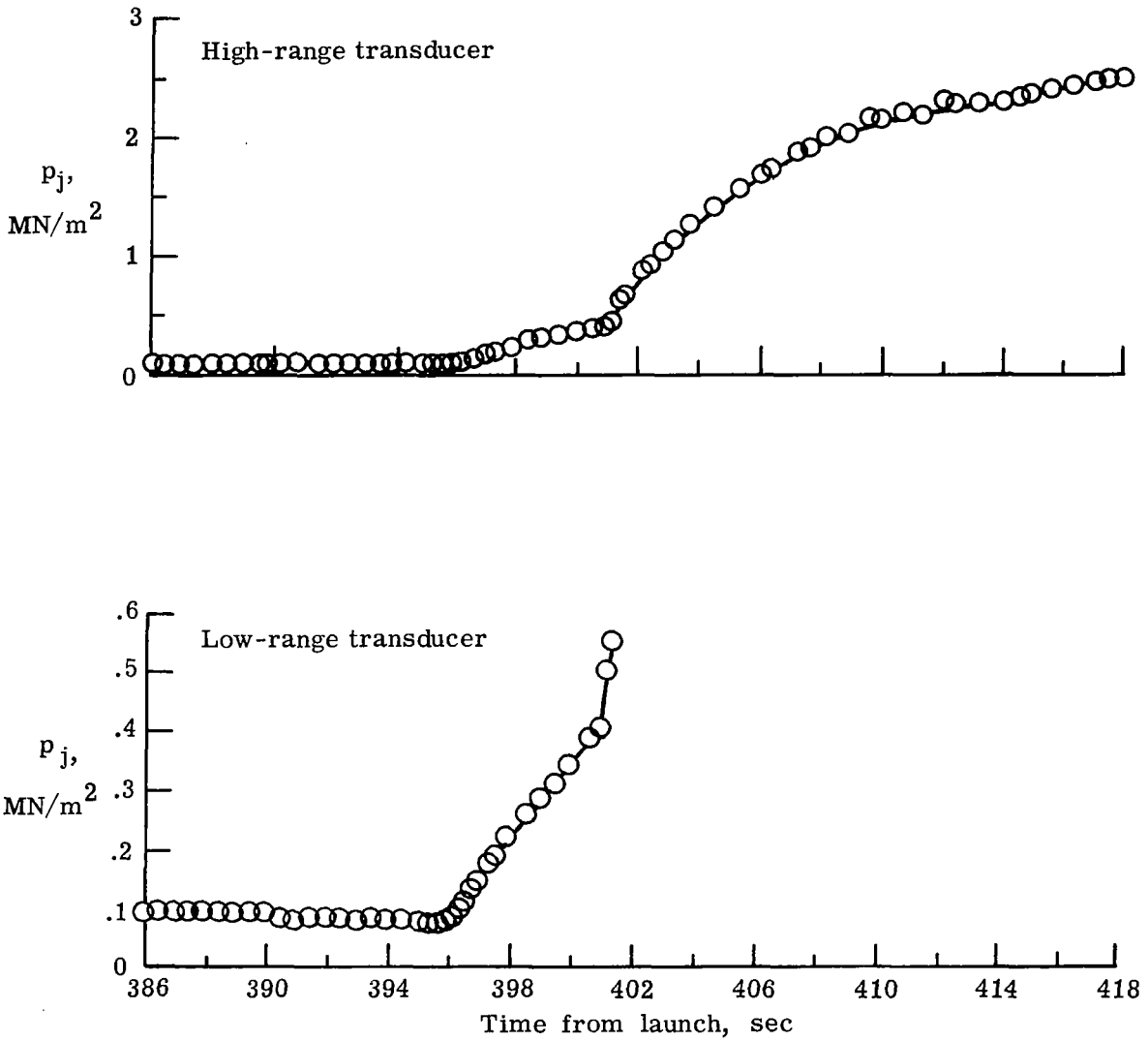


Figure 22.- Liquid-injection pressure measured on RAM C-III flight.

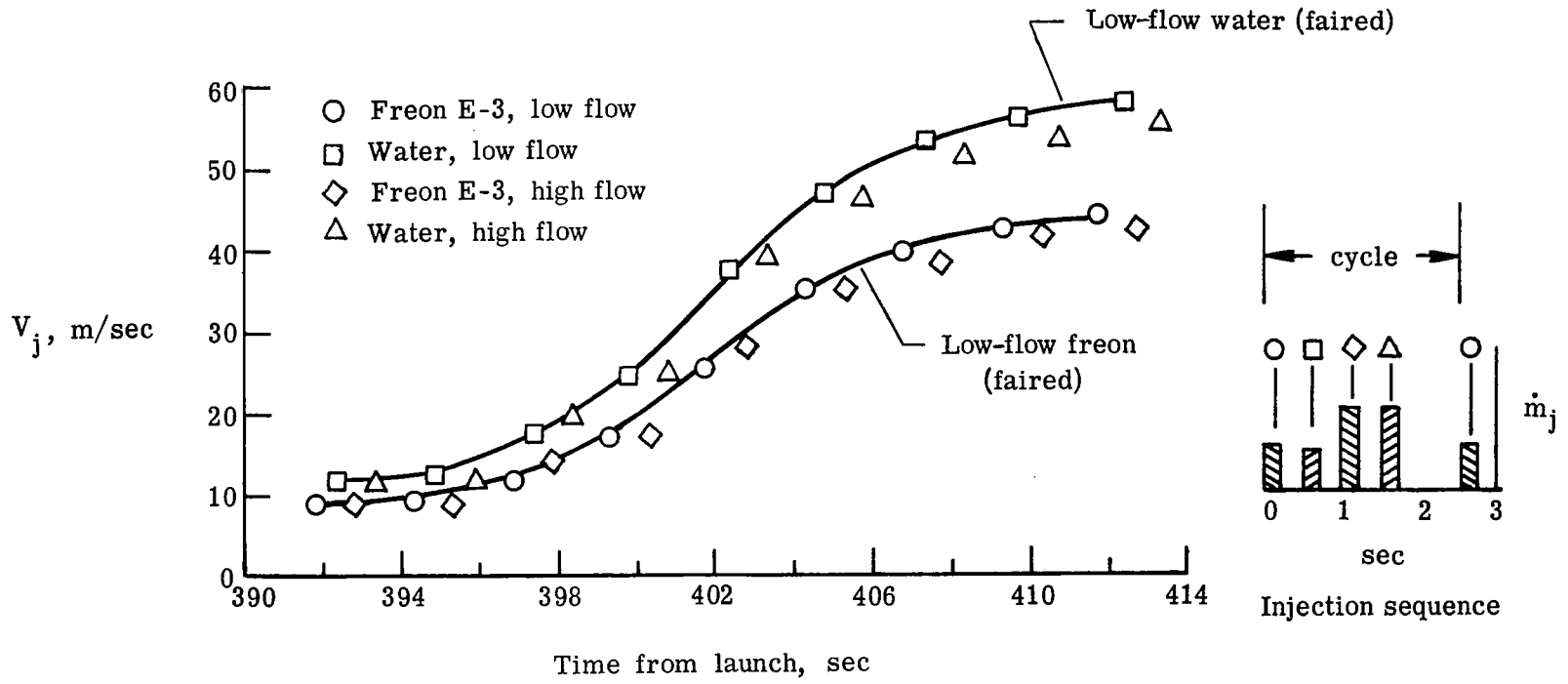


Figure 23.- Computed liquid-injection velocity for the RAM C-III flight experiment.

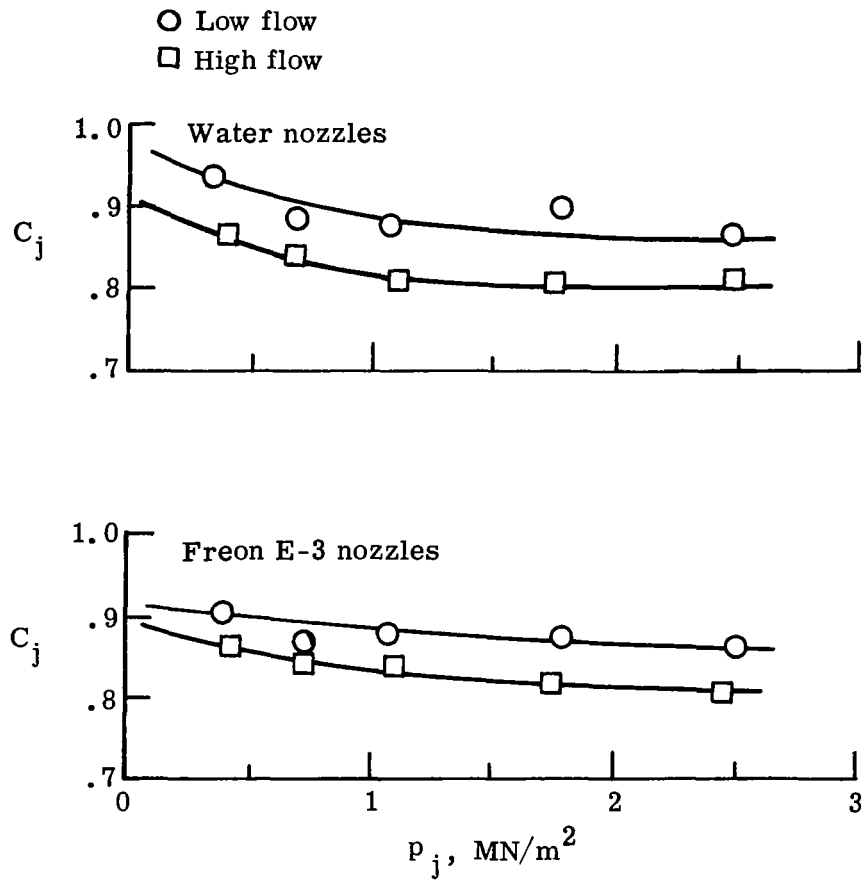


Figure 24.- RAM C-III flight injection nozzles discharge coefficients.

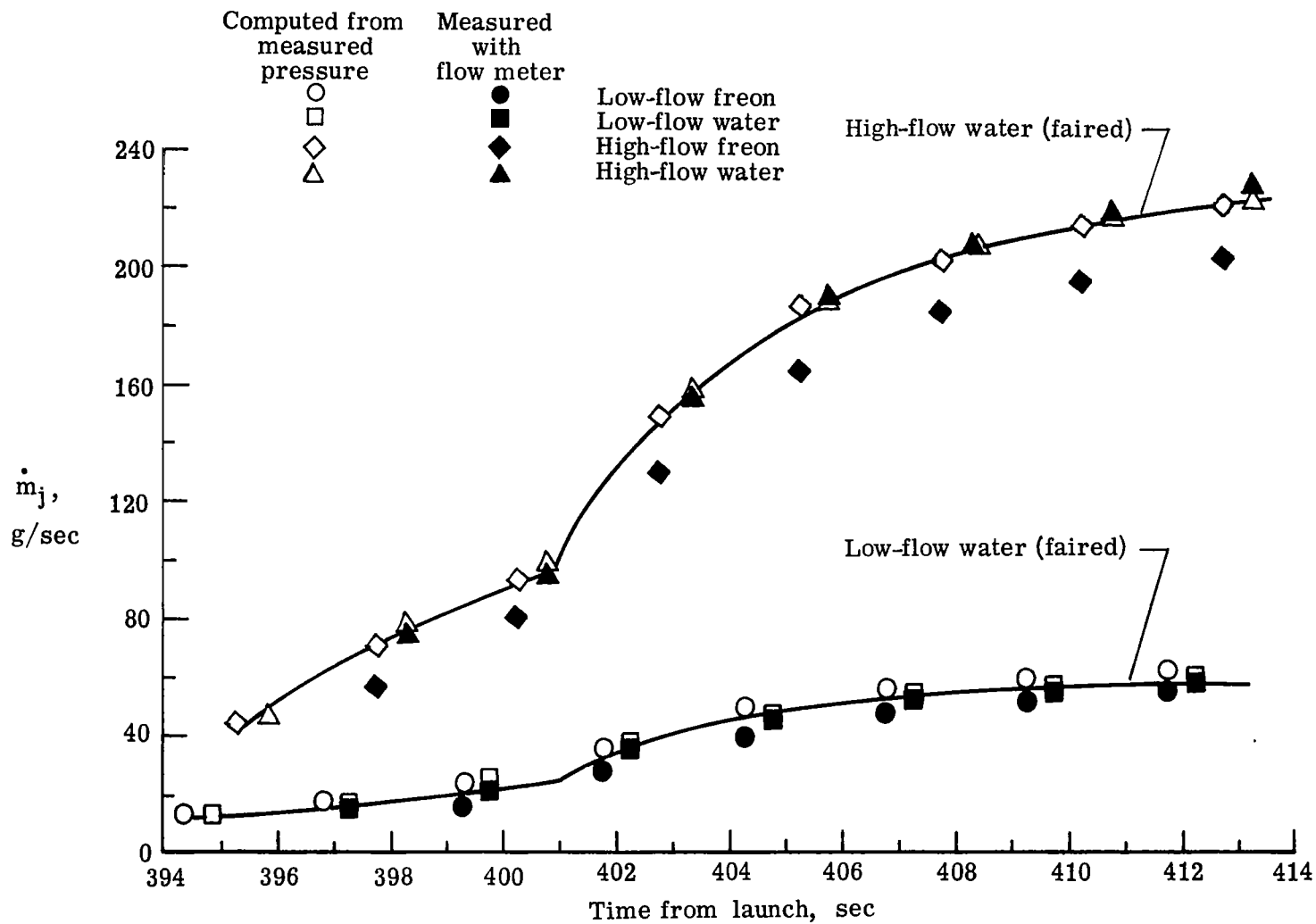


Figure 25.- Comparison of measured and computed liquid-flow rates for RAM C-III flight.

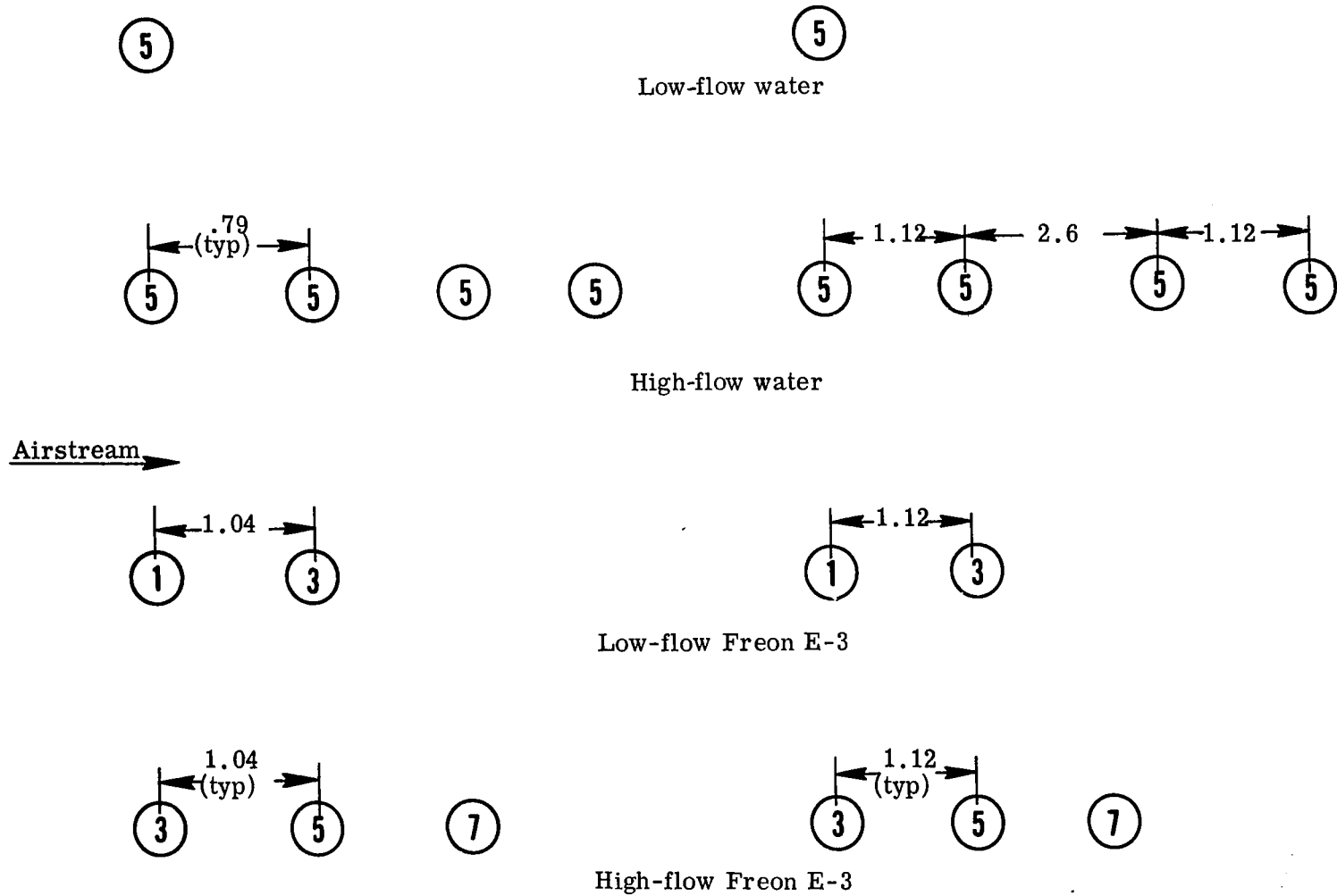


Figure 26.- Comparisons of nozzle spacing for RAM C-III tests and flight nozzles.
All dimensions in centimeters; numbers in circles denote orifices.

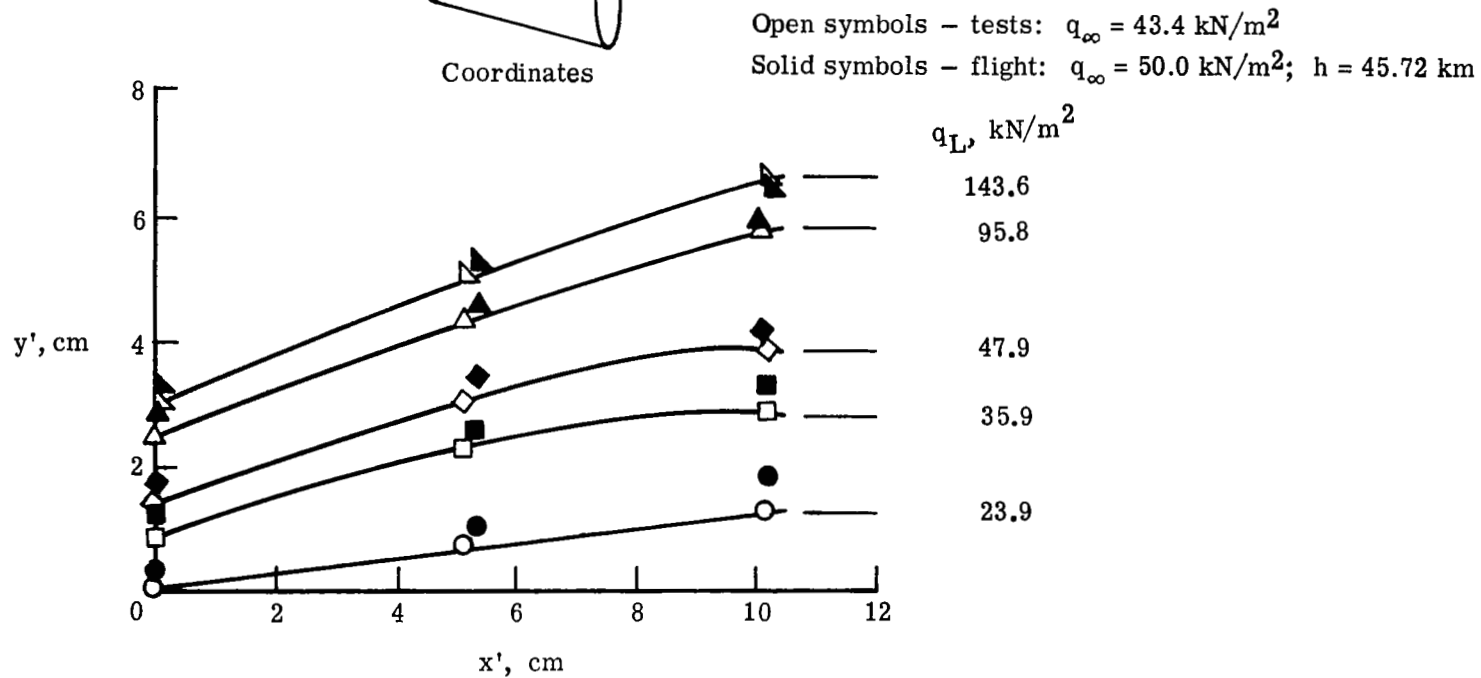
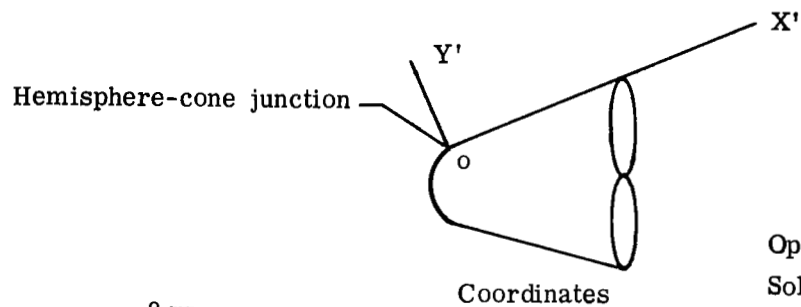


Figure 27.- Lines of constant dynamic pressure in flow fields of hemisphere-cone test model and flight spacecraft.

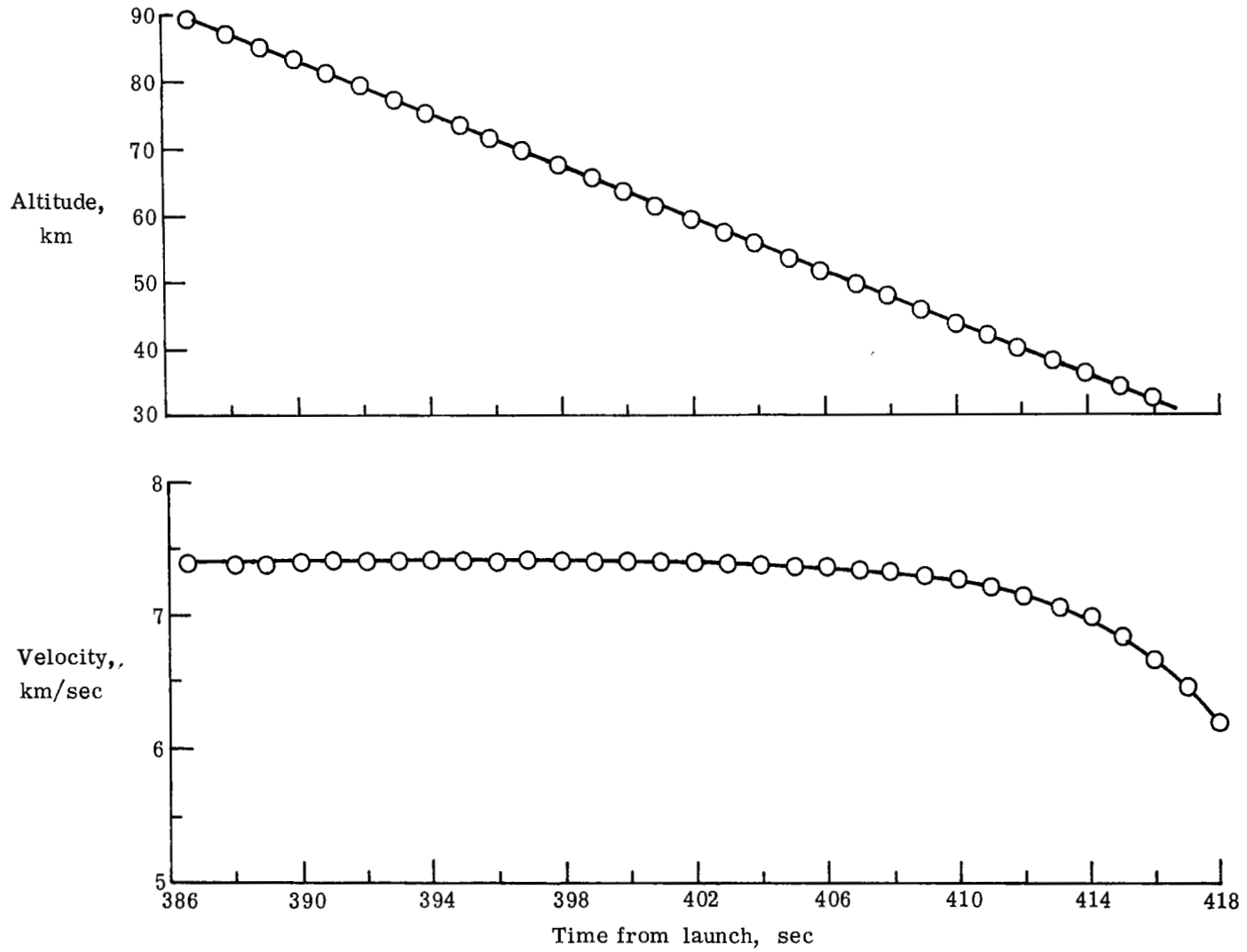


Figure 28.- RAM C-III entry altitude and velocity.

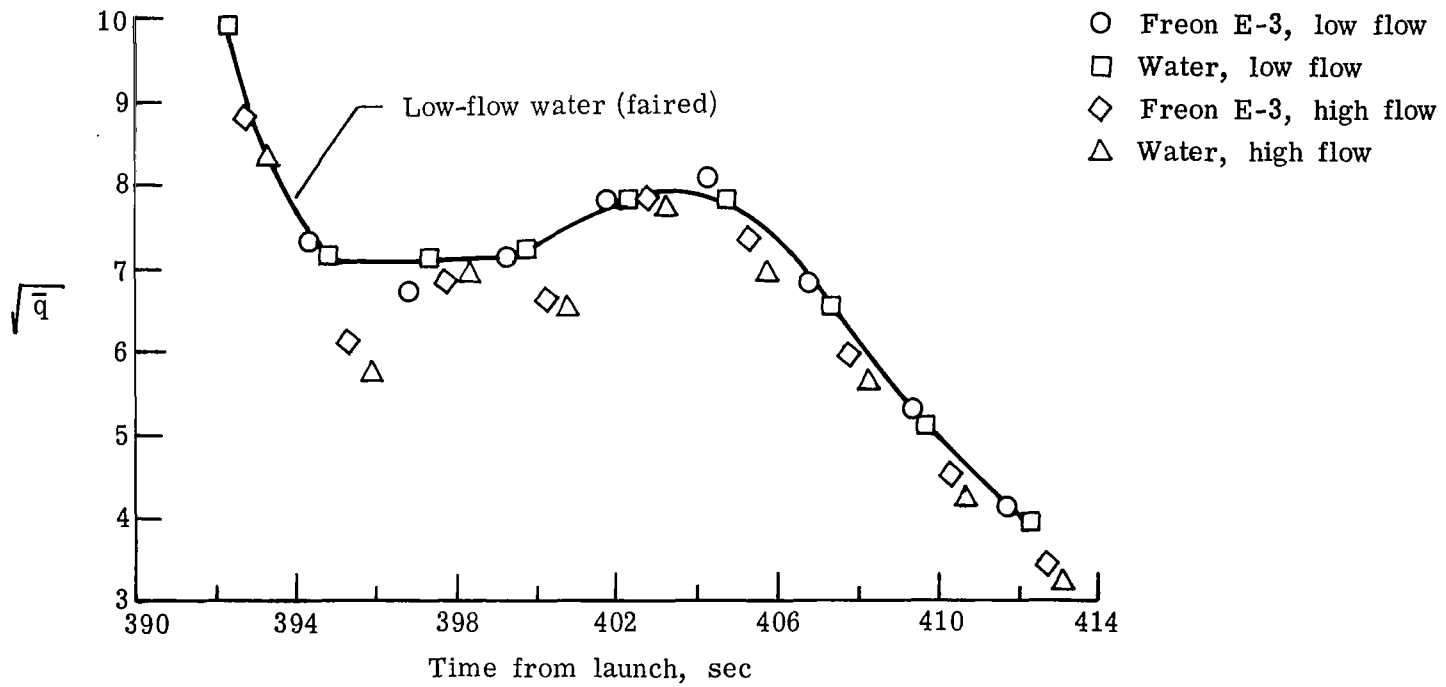


Figure 29.- RAM C-III penetration correlation parameter.

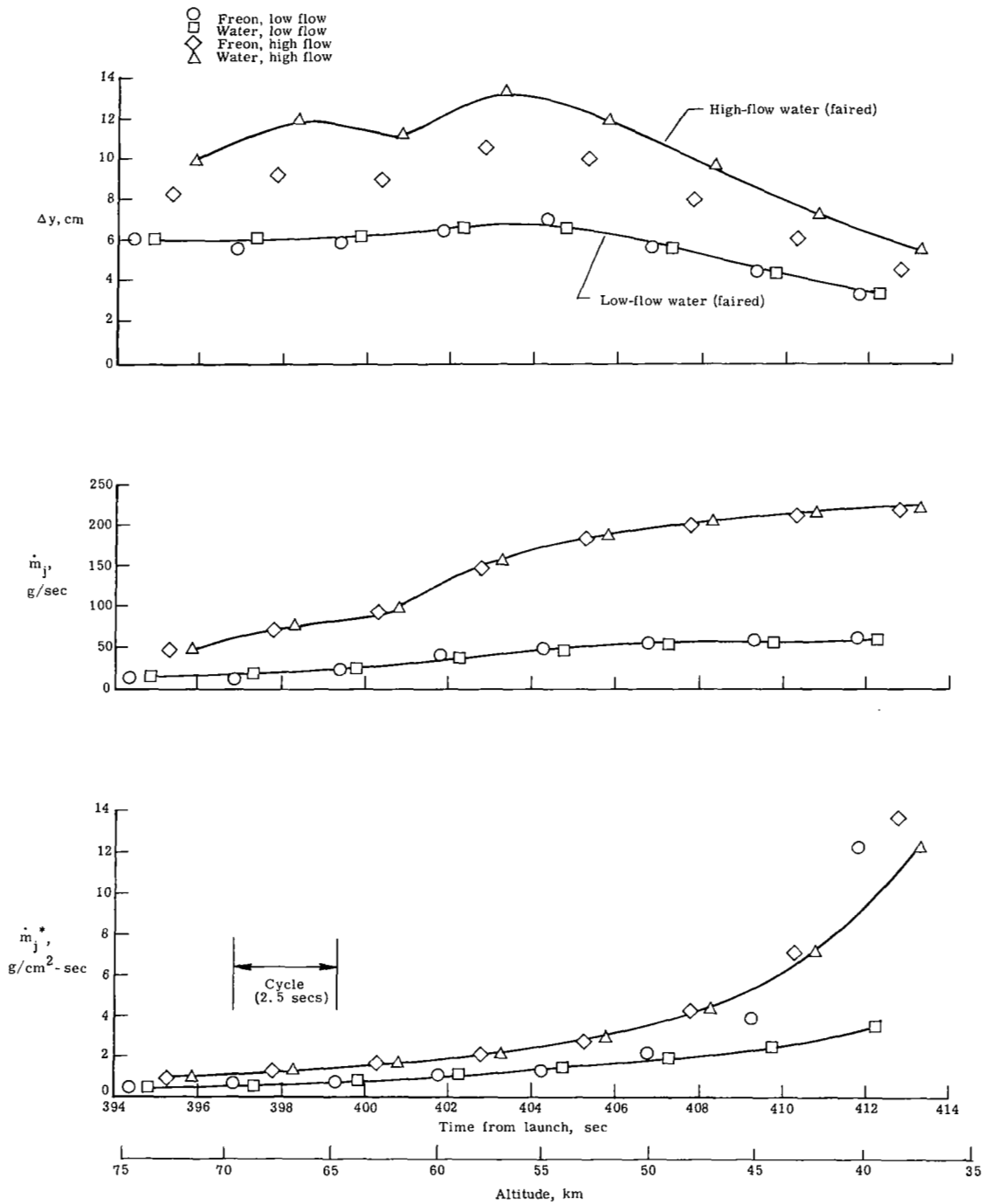


Figure 30.- RAM C-III liquid penetration, flow rate, and flow flux.

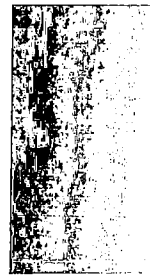
OFFICIAL BUSINESS
PENALTY FOR PRIVATE USE \$300

FIRST CLASS MAIL

POSTAGE AND FEES PAID
NATIONAL AERONAUTICS AND
SPACE ADMINISTRATION



024B 01 C2 UL 01 720121 S00903DS 720401
DEPT OF THE AIR FORCE
AF WEAPONS LAB (AFSC)
TECH LIBRARY/WLOL/
ATTN: E LOU BOWMAN, CHIEF
KIRTLAND AFB NM 87117



POSTMASTER: If Undeliverable (Section 158
Postal Manual) Do Not Return

"The aeronautical and space activities of the United States shall be conducted so as to contribute . . . to the expansion of human knowledge of phenomena in the atmosphere and space. The Administration shall provide for the widest practicable and appropriate dissemination of information concerning its activities and the results thereof."

— NATIONAL AERONAUTICS AND SPACE ACT OF 1958

NASA SCIENTIFIC AND TECHNICAL PUBLICATIONS

TECHNICAL REPORTS: Scientific and technical information considered important, complete, and a lasting contribution to existing knowledge.

TECHNICAL NOTES: Information less broad in scope but nevertheless of importance as a contribution to existing knowledge.

TECHNICAL MEMORANDUMS: Information receiving limited distribution because of preliminary data, security classification, or other reasons.

CONTRACTOR REPORTS: Scientific and technical information generated under a NASA contract or grant and considered an important contribution to existing knowledge.

TECHNICAL TRANSLATIONS: Information published in a foreign language considered to merit NASA distribution in English.

SPECIAL PUBLICATIONS: Information derived from or of value to NASA activities. Publications include conference proceedings, monographs, data compilations, handbooks, sourcebooks, and special bibliographies.

TECHNOLOGY UTILIZATION PUBLICATIONS: Information on technology used by NASA that may be of particular interest in commercial and other non-aerospace applications. Publications include Tech Briefs, Technology Utilization Reports and Technology Surveys.

Details on the availability of these publications may be obtained from:

SCIENTIFIC AND TECHNICAL INFORMATION OFFICE

NATIONAL AERONAUTICS AND SPACE ADMINISTRATION

Washington, D.C. 20546